

Population heterogeneity in the epithelial to mesenchymal transition is controlled by NFAT and phosphorylated Sp1

Russell Gould[‡] and David M. Bassen, Anirikh Chakrabarti, Jeffrey D. Varner and Jonathan Butcher^{‡*}

Robert Frederick Smith School of Chemical and Biomolecular Engineering and [‡]Nancy E. and Peter C. Meinig School of Biomedical Engineering, Cornell University, Ithaca NY 14853

Running Title: Modeling of TGF- β induced EMT

Character count: 56,659

*Corresponding author:

Jonathan T. Butcher,

Associate Professor, Nancy E. and Peter C. Meinig School of Biomedical Engineering,
304 Weill Hall, Cornell University, Ithaca NY, 14853

Email: jtb47@cornell.edu

Phone: (607) 255 - 3575

Fax: (607) 255 - 7330

Abstract

Epithelial to mesenchymal transition (EMT) is an essential differentiation program during tissue morphogenesis and remodeling. EMT is induced by soluble transforming growth factor β (TGF- β) family members, and restricted by vascular endothelial growth factor family members. While many downstream molecular regulators of EMT have been identified, these have been largely evaluated individually without considering potential crosstalk. In this study, we created an ensemble of dynamic mathematical models describing TGF- β induced EMT to better understand the operational hierarchy of this complex molecular program. We used ordinary differential equations (ODEs) to describe the transcriptional and post-translational regulatory events driving EMT. Model parameters were estimated from multiple data sets using multiobjective optimization, in combination with cross-validation. TGF- β exposure drove the model population toward a mesenchymal phenotype, while an epithelial phenotype was enhanced following vascular endothelial growth factor A (VEGF-A) exposure. Simulations predicted that the transcription factors phosphorylated SP1 and NFAT were master regulators promoting or inhibiting EMT, respectively. Surprisingly, simulations also predicted that a cellular population could exhibit phenotypic heterogeneity (characterized by a significant fraction of the population with both high epithelial and mesenchymal marker expression) if treated simultaneously with TGF- β and VEGF-A. We tested this prediction experimentally in both MCF10A and DLD1 cells and found that upwards of 45% of the cellular population acquired this hybrid state in the presence of both TGF- β and VEGF-A. We experimentally validated the predicted NFAT/Sp1 signaling axis for each phenotype response. Lastly, we found that cells in the hybrid state had significantly different functional behavior when compared to VEGF-A or TGF- β treatment alone. Together, these results establish a predictive mechanistic model of EMT susceptibility, and potentially reveal a novel signaling axis which regulates carcinoma progression through an EMT versus tubulogenesis response.

Author Summary

Tissue formation and remodeling requires a complex and dynamic balance of interactions between epithelial cells, which reside on the surface, and mesenchymal cells that reside in the tissue interior. During embryonic development, wound healing, and cancer, epithelial cells transform into a mesenchymal cell to form new types of tissues. It is important to understand this process so that it can be controlled to generate beneficial effects and limit pathological differentiation. Much research over the past 20 years has identified many different molecular species that are relevant, but these have mainly been studied one at a time. In this study, we developed and implemented a novel computational strategy to interrogate the key players in this transformation process to identify which are the major bottlenecks. We determined that NFATc1 and pSP1 are essential for promoting epithelial or mesenchymal differentiation, respectively. We then predicted the existence of a partially transformed cell that exhibits both epithelial and mesenchymal characteristics. We found this partial cell type develops a network of invasive but stunted vascular structures that may be a unique cell target for understanding cancer progression and angiogenesis.

1 Introduction

2 The epithelial to mesenchymal transition (EMT) is a broadly participating, evolutionarily
3 conserved differentiation program essential for tissue morphogenesis, remodeling and
4 pathological processes such as cancer (Thiery, 2003). During EMT polarized, tightly ad-
5 hered epithelial cell monolayers are transformed into non-interacting motile mesenchymal
6 cells that simultaneously degrade and synthesize extracellular matrix (ECM) components
7 and invade into the underlying tissue space (Stahl & Felsen, 2001). EMT is the funda-
8 mental initiator of developmental processes such as embryonic gastrulation and valvulo-
9 genesis (Eisenberg & Markwald, 1995) (also Kalluri J Clin Invest 2009, Thiery Cell 2009).
10 Transforming growth factor β (TGF- β) family members are important inducers of both de-
11 velopmental and pathological EMT (Xu *et al.*, 2009, Zavadil & Böttinger, 2005). Decades

12 of research has focused on identifying molecular regulators of EMT, but almost all on
13 a single gene and in a nearly binary yes/no level of qualitative understanding. Medici
14 and coworkers identified a core signaling program by which TGF- β isoforms induce EMT
15 across a variety of cell lines (Medici *et al.*, 2006, 2008). This program involves carefully
16 orchestrated rounds of gene expression driven by the Smad and Snail families of tran-
17 scription factors as well as other key factors such as lymphoid enhancer-binding factor 1
18 (LEF-1), nuclear factor of activated T-cells, cytoplasmic 1 (NFATc1), and specificity protein
19 1 (Sp1). Coregulators such as β -catenin, NF- κ B, and the ErbB family of receptor tyrosine
20 kinases however also participate in EMT regulation, but the degree of each's influence is
21 difficult to ascertain in isolation (Hardy *et al.*, 2010, Huber *et al.*, 2004, Jiang *et al.*, 2007,
22 Kim *et al.*, 2002). EMT also exhibits complex temporal dynamics that are often intractable
23 in gain/loss of function studies. Elucidating the master regulatory architecture controlling
24 EMT therefore requires inclusion of these complex overlapping and non-binary behaviors.

25 Systems biology and mathematical modeling are essential tools for understanding
26 complex developmental programs like EMT (Ahmed & Nawshad, 2007). Previous com-
27 putational models of TGF- β induced differentiation focused on single biological factors or
28 EMT in single cells. For example, Chung *et al.*, constructed a model of TGF- β receptor ac-
29 tivation and Smad signaling using ordinary differential equations and mass-action kinetics.
30 Their model suggested that a reduction of functional TGF- β receptors in cancer cells may
31 lead to an attenuated Smad2 signal (Chung *et al.*, 2009). Similarly, Vilar *et al.* suggested
32 that specific changes in receptor trafficking patterns could lead to phenotypes that favor
33 tumorigenesis (Vilar *et al.*, 2006). Although these models provided insight into the role of
34 receptor dynamics, EMT induction involves many other components, including compet-
35 ing second messengers and interconnected transcriptional regulatory loops. Integrating
36 these additional scales of molecular signaling while maintaining the capacity for robust
37 prediction requires a new and expanded computational and experimental strategy. Data-
38 driven systems approaches (Cirit & Haugh, 2012) or logical model formulations (Morris

39 *et al.*, 2011) are emerging paradigms that constrain model complexity through the incor-
40 poration of training and validation data. These are interesting techniques because the
41 data informs model structure (which can be expanded as more data becomes available).
42 Alternatively, Bailey proposed more than a decade ago that a qualitative understanding
43 of a complex biological system should not require complete definition of its structural
44 and parametric content (Bailey, 2001). Shortly thereafter, Sethna and coworkers showed
45 that complex model behavior is often controlled by only a few parameter combinations, a
46 characteristic seemingly universal to multi-parameter models referred to as “sloppiness”
47 (Machta *et al.*, 2013). Thus, reasonable model predictions are often possible with only
48 limited parameter information. Taking advantage of this property, we developed sloppy
49 techniques for parameter identification using ensembles of deterministic models (Song
50 *et al.*, 2010). Furthermore, we proposed that the sloppy behavior of biological networks
51 may also be seen as a source of cell-to-cell (Lequieu *et al.*, 2011) or even patient-to-
52 patient heterogeneity (Luan *et al.*, 2010). Bayesian parameter identification techniques
53 have also been used to explore cell-to-cell heterogeneity (Hasenauer *et al.*, 2011, Kalita
54 *et al.*, 2011), where a population of cells could be viewed as a dynamic ensemble of
55 context-specific biochemical networks (Creixell *et al.*, 2012).

56 In this study, we developed a family of mathematical models describing the induction
57 of EMT by TGF- β isoforms in the presence and absence of vascular endothelial growth
58 factor A (VEGF-A). We integrated a simple rule-based description of activity and gene
59 expression regulation with traditional ordinary differential equation (ODE) modeling to de-
60 scribe an EMT interaction network containing 97 gene, protein or mRNA components in-
61 terconnected through 169 interactions. This integration allows the description of complex
62 regulatory interactions in the absence of specific mechanistic information, it also allowed
63 to build a predictive yet compact model. A family of model parameters was estimated
64 using 41 molecular data sets generated in DLD1 colon carcinoma, MDCKII and A375
65 melanoma cells using the Pareto optimal ensemble technique (JuPOETs) multiobjective

optimization algorithm. JuPOETs generated an ensemble of approximately 1400 models for analysis. Analysis of the model population suggested that both MCF10A and DLD1 cells could exhibit phenotypic heterogeneity if treated simultaneously with TGF- β 1/2 and VEGF-A. This heterogeneity was characterized by a significant fraction of the population being in a “hybrid state” having both high E-cadherin and high Vimentin expression. We tested these predictions using qRT-PCR and flow-cytometry studies in a variety of experimental conditions. Validation studies confirmed that upwards of 45% of the cellular population could be put into the hybrid state in the presence of both TGF- β 1/2 and VEGF-A. Moreover, this response depended upon both activation of Sp1 by MAPK and NFATc1 transcriptional activity consistent with the predicted molecular signaling. Lastly, the hybrid populations of both DLD1 and MCF10A cells exhibited different functional behavior than those from either TGF- β or VEGF-A treatment. The extent of ductal branch formation significantly increased with MCF10A cells in the hybrid phenotype, compared with cells treated with VEGF-A alone. Together, these results establish a predictive mechanistic model of EMT susceptibility, and reveal a novel signaling axis, which possibly regulates carcinoma progression through an EMT versus tubulogenesis response.

82 **Results**

83 **The model population captured key features of TGF- β induced EMT** The EMT model
84 architecture, based upon curated molecular connectivity, described the expression of 23
85 genes following exposure to TGF- β isoforms and VEGF-A (Fig. 1). The EMT model
86 contained 74 molecular species interconnected by 169 interactions. Model equations
87 were formulated as ordinary differential equations (ODEs) augmented with rule-based de-
88 scriptions of activity and gene expression regulation. ODEs are common tools to model
89 biochemical pathways (Chen *et al.*, 2009, Schoeberl *et al.*, 2002, Tasseff *et al.*, 2011).
90 However, while ODE models can simulate complex intracellular behavior, they require
91 estimates for model parameters which are often difficult to obtain. The EMT model had
92 251 unknown model parameters, 169 kinetic constants 38 control constants and 44 sat-
93 uration constants. As expected, these parameters were not uniquely identifiable given
94 the training data (Gadkar *et al.*, 2005). Thus, instead of identifying a single best fit (but
95 uncertain) model, we estimated a sloppy population of models (each consistent with the
96 training data) by simultaneously minimizing the difference between model simulations and
97 41 molecular data sets using the Pareto Optimal Ensemble Technique (JuPOETs). The
98 training data were generated in DLD1 colon carcinoma, MDCKII, and A375 melanoma
99 cells following exposure to TGF- β isoforms (Medici *et al.*, 2008). We organized these
100 data sets into 11 objective functions which were simultaneously minimized by JuPOETs.
101 Additionally, we used data generated in this study (Fig. S4), and 12 molecular data sets
102 generated in HK-2 cells following VEGF-A exposure to train VEGF-A responsive model
103 processes (Lian *et al.*, 2011). To guard against overfitting, we augmented the multiobjec-
104 tive optimization with leave-one-out cross validation to independently estimate both the
105 training and prediction error for each objective. Thus, we generated 11 different model
106 ensembles. Lastly, we compared model predictions with independent data sets not used
107 during training (both at the molecular and model population levels) to evaluate the predic-
108 tive power of the parameter ensemble.

JuPOETs generated a population of probable signaling models which captured the multiple phases of EMT induction (Fig. 2). JuPOETs sampled well over 10^4 probable models during each stage of the cross-validation using global random sampling. From this analysis, $N \simeq 1400$ models were selected for further analysis. The selected models all had the same possible molecular connectivity, but different values for model parameters. Transcription and translation rates, as well as mRNA and protein degradation terms, were set using physical values from the literature (Milo *et al.*, 2010), and allowed to vary by a scaling factor, see methods. Model selection was based upon Pareto rank, the prediction and training error across all objectives. The model population recapitulated key signaling events following TGF- β exposure. We subdivided the response to TGF- β exposure into two phases. First, TGF- $\beta 1/2$ signaling initiated a program which downregulated E-cadherin expression in a MAPK dependent manner while simultaneously upregulating TGF- $\beta 3$ expression. Second, TGF- $\beta 3$ secretion initiated an autocrine feedback which upregulated the expression of mesenchymal markers such as Vimentin and key upstream transcription factors such as LEF-1 in a SMAD dependent manner. TGF- $\beta 3$ expression was also able to sustain β -catenin release by inhibiting its sequestration by the APC complex through PI3K mediated GSK3, which was captured by the model (Fig. 4B). Each phase involved the hierachal expression and/or post-translational modification of several key transcription factors. During the first phase, stimulation with TGF- $\beta 1/2$ (10 a.u.) activated both the SMAD and MAPK pathways. MAPK activation resulted in the phosphorylation of the transcription factor activator protein 1 (AP-1), which in-turn upregulated the expression of Snail, a well established transcriptional repressor (Fig. 2A). Snail expression was MAPK-dependent; the MEK inhibitor U0126 blocked AP-1 activation and Snail expression following TGF- $\beta 1/2$ exposure (Fig. 2A, Lane 3). Similar results were obtained for Slug expression, confirming initial activation through the MAPK pathway (data not shown). Overexpression of either Snail or Slug upregulated TGF- $\beta 3$ expression (Fig. 2C) while simultaneously downregulating E-cadherin expression (Fig. 2F). During the

136 second phase, TGF- β 3 secretion and the subsequent autocrine signaling resulted in the
137 upregulation of mesenchymal marker expression. The TGF- β 3 induced gene expres-
138 sion program involves a complex hierarchy of transcriptional and post-translational reg-
139 ulatory events. Absence of E-cadherin indirectly promoted TGF- β 3 expression through
140 the β -catenin/TCF4 complex following Snail or Slug expression (Fig. 2C, Lane 2 or 3).
141 Conversely, over-expression of E-cadherin inhibited the TGF- β 3 autocrine production by
142 sequestering cytosolic β -catenin, thereby blocking EMT (Fig. 2C, Lane 4 or 5). TGF- β 3
143 signaled through the Smad pathway to regulate LEF-1 expression and downstream tar-
144 get EMT genes (Fig. 2G). TGF- β 3 (10 a.u.) in combination with downstream inhibitors
145 (DN-Smad4 and DN-LEF-1) completely inhibited Vimentin expression, while elevating E-
146 cadherin expression (Fig. 2H,I).

147 The predictive power of the ensemble was tested using cross validation and by com-
148 paring simulations with data not used for model training. In whole, all of our training
149 objectives were statistically significant (at a 95% confidence interval) compared to a ran-
150 domized parameter family ($N = 100$) generated from a random starting point. Conversely,
151 we *predicted* all of the training objectives, at a 95% confidence interval compared to ran-
152 domized parameters (Wicoxon non-parametric test). The model also captured the tem-
153 poral gene expression responses of E-cadherin, pSmad2, and LEF-1 (not used for model
154 training) to within one-standard deviation (up to the 48 hr time-point) (Fig. 2J-L). Taken
155 together, the model captured the key signaling events revealed by Medici *et al.* (Medici
156 *et al.*, 2008) that drive the phenotypic conversion. A listing of objective function values
157 resulting from training, cross validation and the random parameter control is given in the
158 supplement (Fig. S1).

159 **Identification of a novel LEF-1 regulator** During model identification, we found that
160 consistent TGF- β induced EMT from a stable epithelial cell population required an addi-
161 tional regulatory protein. This protein, which we called hypothetical regulator 1 (YREG1),
162 was required to mediate between SNAIL/SLUG transcriptional activity and the upregu-

lation of LEF-1 expression following TGF- β 1/2 exposure. SNAIL/SLUG are well known transcriptional repressors (Dhasarathy *et al.*, 2011, Hemavathy *et al.*, 2000a,b), although there are a few studies which suggest that at least SNAIL can also act as a transcriptional activator (Guaita *et al.*, 2002). In the model, we assumed the expression of SNAIL/SLUG was likely regulated by AP1/SP1 (Jackstadt *et al.*, 2013). Thus, upon receiving direct SNAIL/SLUG and TGF- β 3 signals, the model predicted enhanced SNAIL/SLUG expression, consistent with experimental observations. TGF- β 1/2 stimulation also induces LEF-1 expression. However, literature evidence suggested that LEF-1 expression was not strongly dependent upon AP1/SP1 activity (Eastman & Grosschedl, 1999). Thus, either SNAIL/SLUG are acting as inducers (contrary to substantial biochemical evidence) or, they are repressing the expression of an intermediate repressor. Given the biochemical evidence supporting SNAIL/SLUG as repressors, we created the hypothetical YREG1 repressor whose expression is downregulated by SNAIL/SLUG. The literature data therefore suggested that YREG1 had two transcriptional targets, LEF-1 and TGF- β 3. By adding this regulator, our simulations became consistent with training and literature data. Medici *et al.* suggested that feedback between β -catenin and LEF-1 was likely, although this feedback had yet to be identified (Medici *et al.*, 2008). Low levels of YREG1 expression were present in all simulations to regulate the formation of the β -catenin-LEF-1 complex. To test the effect of YREG1 on the epithelial population, we conducted over-expression and knockdown simulations on untreated cells (Fig. 4C and 4D). In the absence of YREG1, the population of models failed to consistently retain a stable epithelial state (Fig. 4D). Conversely, YREG1 amplification revealed an enhanced epithelial phenotype, while some inherently transformed cells moved towards a hybrid phenotype (Fig. 4C). Elevated YREG1 repressed LEF-1 and TGF- β 3 expression, thereby not allowing free β -catenin to form the β -catenin-LEF-1 complex, or TGF- β 3 induced SMAD activation. Taken together, low YREG1 expression was required for the maintenance of a stable epithelial phenotype that was simultaneously inducible across TGF- β 1/2, TGF- β 3 and SNAIL/SLUG transfection.

190 **TGF- β 1/2 and VEGF-A exposure promotes phenotype heterogeneity through NFATc
191 and phosphorylated Sp1** While we captured the central tendency of many of the molec-
192 ular features of EMT induction following TGF- β 1/2 exposure, an often neglected but im-
193 portant emergent feature of developmental and pathological programs is population het-
194 erogeneity (Park *et al.*, 2010). We (and others) have previously hypothesized that deter-
195 ministic model ensembles can simulate population behavior, at least at a course grained
196 level (Lequieu *et al.*, 2011). We tested this hypothesis by analyzing the response of the
197 population of EMT models to extracellular cues and then comparing this response to flow
198 cytometry studies. We quantified the phenotypic response of the individual members of
199 the ensemble to TGF- β 1/2 stimulation for two downstream phenotypic markers, Vimentin
200 (mesenchymal) and E-cadherin (epithelial) following the addition of TGF- β 1/2 alone (Fig.
201 3), and/or VEGF-A in combination with NFATc inhibitors (Fig. 3).

202 We identified model subpopulations that exhibited different behaviors following expo-
203 sure to TGF- β 1/2 (Fig. 3B). Analysis of the molecular signatures of these subpopulations
204 suggested the abundance, localization and state of the Sp1, AP-1 and NFATc transcription
205 factors controlled population heterogeneity. The majority of models (>80%) responded
206 to treatment, moving away from the untreated population (Fig 3A-F, gray). These mod-
207 els showed the classically expected behavior, a switch from an epithelial to mesenchy-
208 mal phenotype following TGF- β 1/2 exposure. Some models resembled untreated cells;
209 they had elevated phosphorylated Sp1, relative to non-induced cells, which decreased E-
210 cadherin expression through Slug-mediated inhibition, which in turn increased Vimentin
211 expression through TGF- β 3 autocrine signaling and the liberation of β -catenin. How-
212 ever, the most biologically interesting behavior was exhibited by cells achieving a hybrid
213 phenotype, most notable in a dual treatment condition (3C, black arrow), but also present
214 in a small percentage of untreated cells (Fig. 3B, gray arrow). Models with this hybrid
215 phenotype had elevated Sp1 and NFAT transcriptional activity, resulting in simultaneously
216 increased Vimentin and E-cadherin expression (Fig. 4A).

217 To better understand the hybrid phenotype, we simulated the response of the model
218 population to TGF- β 1/2 and VEGF-A treatment with and without NFATc inhibitors (Fig.
219 3). As expected, stimulation with VEGF-A (50 a.u.) maintained an epithelial population
220 (Fig. 3A), while TGF- β 1/2 (10 a.u.) exposure shifted the population from an epithelial
221 to a mesenchymal phenotype (Fig. 3B). On the other hand, combined stimulation with
222 TGF- β 1/2 (10 a.u.) and VEGF-A (50 a.u.) increased both E-cadherin and Vimentin ex-
223 pression, resulting in a hybrid phenotype with both epithelial and mesenchymal character-
224 istics (Fig. 3C). Vimentin expression was correlated with high levels of nuclear phospho-
225 rylated Sp1, following TGF- β 1/2 exposure. Conversely, elevated E-cadherin expression
226 depended upon the activity of NFAT transcription factors downstream of VEGF-A stimula-
227 tion. To further isolate the role of NFAT on this hybrid state, we simulated the inhibition of
228 NFAT transcriptional activity across all conditions (all else being equal). NFAT inhibition
229 in combination with VEGF-A or TGF- β 1/2 treatments blocked increased E-cadherin ex-
230 pression in the case of VEGF-A (Fig. 3D), but did not influence TGF- β 1/2 signaling (Fig.
231 3E). Lastly, NFATc inhibition in combination with simultaneous TGF- β 1/2 and VEGF-A
232 exposure repressed nearly all E-cadherin expression, shifting nearly the entire population
233 towards a mesenchymal phenotype (Fig. 3F). Taken together, high levels of nuclear local-
234 ized phosphorylated Sp1 correlated with Vimentin expression, while NFATc transcriptional
235 activity was critical for maintaining E-cadherin expression in the presence of competing
236 signals.

237 **Combined TGF- β 2 and VEGF-A exposure drives heterogeneity in MCF10A and**
238 **DLD1 cells** The EMT model simulations suggested the transcriptional activity of NFATc
239 and Sp1 could be independently tuned to generate a hybrid cell population with both
240 epithelial and mesenchymal characteristics. To test this hypothesis, we exposed either
241 quiescent epithelial (MCFA10, Fig. 5) or transformed epithelial cells (DLD1, Fig. S2) to
242 combinations of TGF- β 1/2 and/or VEGF-A. As expected, TGF- β 1/2 treatment (10ng/ml)
243 increased Slug and Vimentin expression, while repressing E-cadherin expression both at

the transcript and protein levels in MCF10A (Fig. 5A-B) and DLD1 cells (Fig. S3C). Both MCF10A (Fig. 5C) and DLD1 cells (Fig. S2E,G) transitioned from quiescent cobble-stone morphology to spread spindle shapes, consistent with EMT. As predicted, we found increased nuclear localization of phosphorylated Sp1 following TGF- β 1/2 stimulation in both MCF10A (Fig. 5B,C) and DLD1 cells (Fig. S2E,F). Consistent with model predictions, VEGF-A (50ng/ml) treatment increased the abundance of NFATc1 and E-cadherin at both the transcript and protein level in both MCF10A (Fig. 5A) and DLD1 cells (Fig. S2). We also found that NFATc1 nuclear localization significantly increased in both MCF10 (Fig. 5B,C) and DLD1 (Fig. S2C,E) cells treated with VEGF-A. Interestingly, combining VEGF-A (50ng/ml) with TGF- β 1/2 (10ng/ml) resulted in significantly elevated expression of both E-cadherin and Vimentin at the transcript and protein levels in both MCF10A (Fig. 5A,B) and DLD1 cells (Fig. S2-S3). NFATc1 expression increased, while Sp1 expression was similar to the TGF- β 1/2 case alone (Fig. 5A-B and Fig. S2D,E), supporting their independent regulation. The expression of Slug, and Vimentin significantly increased, while E-cadherin levels were increased in MCF10A cells (Fig. 5A) and maintained at control levels in DLD1 cells (Fig. S2D). As predicted, nuclear co-localization of both NFATc1 and phosphorylated Sp1 were apparent in MCF10A (Fig. 5B,C) and DLD1 (Fig. S2E,F) cells treated with both ligands. Taken together, combined VEGF-A and TGF- β 1/2 treatment elicited a hybrid phenotype expressing both mesenchymal and epithelial characteristics in both MCF10A and DLD1 cells. This phenotype was driven by the transcriptional activity of two key transcription factors, Sp1 and NFATc, which could be modulated independently by TGF- β 1/2 and VEGF-A exposure.

Our phenotypic analysis predicted that NFATc transcriptional activity was critical to maintaining E-cadherin expression in the presence of both VEGF-A and TGF- β 1/2. We experimentally tested this hypothesis by exposing both MCF10A (Fig. 5E,F) and DLD1 cells (Fig. S3) to combinations of VEGF-A and TGF- β 1/2 in the presence or absence of VIVIT, a soluble peptide inhibitor of NFATc transcriptional activity (Aramburu *et al.*,

271 1999). Treatment with VEGF-A (50ng/ml) and VIVIT (10 μ M) in MCF10A cells significantly
272 reduced E-cadherin expression compared to VEGF-A alone (Fig. 5D,E). Co-treatment
273 with VIVIT and TGF- β 1/2 did not enhance EMT capacity of MCF10A cells above that
274 of TGF- β 1/2 alone (Fig. 5A,B,E). Likewise, VIVIT in combination with both TGF- β 1/2
275 and VEGF-A resulted in a loss of E-cadherin gene and protein expression, while Slug
276 and Vimentin levels remained increased (Fig. 5D,E). Quantitative flow cytometry con-
277 firmed these results in both MCF10A (Fig. 5F) and DLD1 cells (Fig. S3C). Both epithelial
278 cell lines initially had high levels of E-cadherin expression, and low Vimentin abundance
279 (Q1-99.5%), but both MCF10A and DLD1 cells shifted from an epithelial to mesenchymal
280 phenotype (Q1-33.4%, Q4-42.8%) following TGF- β 1/2 exposure. As expected, NFATc
281 nuclear localization was repressed with VIVIT treatment regardless of ligand stimulation,
282 while the abundance of nuclear phosphorylated Sp1 increased for both TGF- β 1/2 and
283 TGF- β 1/2 + VIVIT conditions (Fig. 5C,E). Combined TGF- β 1/2 and VEGF-A increased
284 both Vimentin and E-cadherin expression (Q1-42.1%, Q2-52.3%) compared to TGF- β 1/2
285 alone. Together, these results demonstrate that NFATc and phosphorylated Sp1 are criti-
286 cal for regulating E-cadherin and Vimentin expression during phenotype heterogeneity in
287 MCF10A and DLD1.

288 **Ductal branching during acini formation is dependent upon phenotype heterogene-
289 ity in MCF10A and DLD1 cells** We finally employed established three-dimensional
290 (3D) *in vitro* models of invasion, migration, compaction, and tubulogenesis (Dhimolea
291 *et al.*, 2010) to determine the functional consequences of the hybrid phenotype (Fig. 6).
292 MCF10A and DLD1 cells were aggregated via hanging drop, placed on the surface of a
293 collagen gel, and cultured for 72 hrs under various biochemical treatments. TGF- β 1/2
294 stimulation significantly enhanced cell matrix invasion and matrix compaction, while in
295 contrast VEGF-A stimulation promoted surface migration but no invasion or compaction
296 (Fig. 6B-D). Interestingly, combined TGF- β 1/2 and VEGF-A stimulation significantly in-
297 creased cell migration potential above that of VEGF-A alone while maintaining 3D matrix

298 compaction, though with decreased magnitude compared to TGF- β 1/2 alone. Inhibi-
299 tion of NFATc transcriptional activity by VIVIT decreased migration following treatment
300 with VEGF-A alone (Fig. 6B). Co-treatment of VIVIT significantly decreased migration,
301 while complementarily increasing invasion and compaction, when MCF10A cells were
302 stimulated with both VEGF-A and TGF- β 1/2 (Fig. 6B-D). The responses of DLD1 cells
303 followed a similar trend to MCF10A, although the magnitudes of migration, invasion, and
304 compaction were less. Cell circularity within 3D gels strongly and negatively correlated
305 with both invasion and compaction regardless of treatment (Fig. 6E). Circularity refers
306 to the morphology of the cells. In general, a quiescent epithelial cells assumes a circular
307 morphology in culture, while an active mesenchymal cell is highly elongated. The circular-
308 ity index, a common means of quantifying cell morphology, relates cell area to perimeter.
309 A perfect circle has a circularity index equal to 1.0, while a straight line has a circularity
310 index equal to 0.0, see Butcher et al. (Butcher *et al.*, 2004). TGF- β 1/2 treatment alone
311 resulted in irregular and spindle shaped morphology, while VEGF-A exposure promoted
312 round quiescent cells (Fig. 6A). Combined VEGF-A and TGF- β 1/2 promoted morphology
313 between these extremes. VIVIT mediated NFATc inhibition significantly reduced the cir-
314 cularity index, similar to TGF- β 1/2 treatment (Fig. 6F). VEGF-A treatment also induced
315 the formation of tubular structures (acini), but the number of tubular branches relative to
316 total acini was significantly increased upon combined TGF- β 1/2 and VEGF-A. No tubular
317 structures were identified within the DLD1 constructs during the 7 day tubulogenesis end-
318 points, supporting that MCF10A and DLD1 cells have some cell-type specific EMT sensi-
319 tivity despite their underlying competency for acquiring a heterogeneous phenotype. This
320 suggests that initial EMT sensitivity of a cell influences downstream functional response
321 from TGF- β and VEGFA stimulation. Together, these results establish that VEGF-A and
322 TGF- β 1/2 ligand concentrations potentiate between acini and ductal branch formation in
323 3D culture, and are dependent upon NFATc activity.

324 **Discussion**

325 In this study, we developed a family of mathematical models describing the induction of
326 EMT by TGF- β isoforms in the presence and absence of VEGF-A. The model, which con-
327 tained 74 molecular species interconnected by 169 interactions, described the expression
328 of 23 genes in response to growth factor stimulation. We estimated an ensemble of likely
329 model parameters using the JuPOETs multiobjective optimization framework. The model
330 population was trained and cross-validated to prescribe biological significance using 41
331 data sets generated in DLD1 colon carcinoma, MDCKII, and A375 melanoma cell lines
332 (Medici *et al.*, 2008). Analysis of this population predicted possible phenotypic modes
333 (and their associated signaling) that cells could exhibit when stimulated with TGF- β and/or
334 VEGF-A. The most novel hypothesis generated from the analysis was that cells could op-
335 erate in a hybrid state defined by both epithelial and mesenchymal traits when stimulated
336 simultaneously with TGF- β and VEGF-A. We tested this hypothesis in MCF10A and DLD1
337 cells stimulated with combinations of TGF- β and VEGF-A. As expected, in the presence
338 of TGF- β or VEGF-A alone, MCF10A and DLD1 cells were either mesenchymal or ep-
339 ithelial, respectively. However, with both TGF- β and VEGF-A, MCF10A and DLD1 cells
340 exhibited a hybrid phenotype, having both epithelial and mesenchymal characteristics.
341 Furthermore, we found that functional traits such as tubulogenesis and ductal branch-
342 ing were different for cells in this hybrid phenotype. Together, this study established a
343 predictive model of EMT induction, determined that deterministic model ensembles could
344 predict population heterogeneity, and proved the existence of a unique hybrid phenotype
345 resulting from the simultaneous integration of extracellular growth factor signals.

346 Cells routinely process a multitude of signals simultaneously, especially when coordi-
347 nating developmental or pathological programs. For example, oncogenic cells integrate
348 both mechanical and chemical cues in their local microenvironment during tumorigenesis,
349 including cytokines VEGF and TGF- β (Hong *et al.*, 2013). VEGF-A mediates patholog-
350 ical angiogenic remodeling of tumors (Nagy *et al.*, 2007), while TGF- β can elicit both

protective and oncogenic responses (Ferrara, 2002, Willis & Borok, 2007). While much research has tested signaling pathways individually, far less is understood about combinatorial stimulation, such as with both VEGF-A and TGF- β . Both *in vitro* and *in vivo* studies have suggested that epithelial cells can exhibit heterogeneous phenotypes in addition to classically defined epithelial or mesenchymal states (Polyak & Weinberg, 2009, Strauss *et al.*, 2011). For example, expression profiling in human epithelial cancer cell lines demonstrated a spectrum of phenotypes, including some that expressed both E-cadherin and Vimentin simultaneously (Neve *et al.*, 2006, Welch-Reardon *et al.*, 2014). Zajchowski *et al.*, speculated that these expression profiles were somehow important for maintaining epithelial properties, while simultaneously allowing other functional behavior such as proliferation and migration (Zajchowski *et al.*, 2001). Whether and how heterogeneous phenotypes arise and participate in cancer progression, as well as their response to pharmacological inhibition are fundamental questions that should receive increased attention. In this study, we determined that a hybrid phenotype could be obtained through combined treatment with VEGF-A and TGF- β , both common factors localized in the tumor microenvironment. Furthermore, our systematic simulation-experimentation strategy identified that the transcriptional activity of Sp1 and NFATc were the critical factors controlling this phenotypic heterogeneity. Several studies have highlighted the importance of NFATc as a key transcription factor involved in cell growth, survival, invasion, angiogenesis and cancer (Mancini & Toker, 2009). For example, proliferation and anchorage-independent growth of pancreatic tumor cells is dependent on calcineurin and NFATc1 activity, consistent with the high levels of nuclear NFATc1 found in pancreatic tumors (Singh *et al.*, 2010). Likewise, our results found that VEGF-A was a potent inducer of NFATc1 expression, which may be required for epithelial cell migration and tubulogenesis. Although specific NFATc isoforms were not distinguished in the model, our simulations suggested that NFATc transcriptional activity was capable of maintaining epithelial traits, even during TGF- β induced EMT. Experimentally, we found that E-cadherin expression

378 was dependent upon NFATc dephosphorylation in response to simultaneous VEGF-A and
379 TGF- β 1/2 treatment. Thus, these results support the hypothesis that NFATc activity plays
380 a critical role in maintaining cell-cell contacts, even during partial EMT.

381 Epithelial cells reproduce tissue-like organization when grown in a three-dimensional
382 extracellular matrix (ECM) environment, and therefore are an attractive model to study
383 morphogenic mechanisms. It is well established that MCF10A cells form structures that
384 closely resemble acini (multi-lobed cluster of cells) in three-dimensional *in vitro* cultures
385 (Debnath *et al.*, 2003). It has been postulated that a cellular response reminiscent of
386 partial EMT underlies this process, stimulating further branching and formation of acini
387 (Pearson & Hunter, 2007). Normally well controlled process such as tubulogenesis can
388 be co-opted by cancer cells to break away from a primary lesion and invade through
389 the surrounding stroma (O'Brien *et al.*, 2004). However, by retaining a transient hybrid
390 EMT-like state, clusters of these tube-forming tumor cells can reform at a high rate af-
391 ter invasion, possibly explaining why invasive human carcinomas frequently appear to be
392 cellular collections with varying degrees of gland-like differentiation (Debnath & Brugge,
393 2005). In this study, we showed that our predicted hybrid phenotype generated by simu-
394 taneous treatment of epithelial cells with VEGF-A and TGF- β possessed altered migra-
395 tion and invasion, which enhanced tubular branching. A salient feature of this behavior,
396 however, was the retention of cell-cell contacts that allowed cells to migrate without com-
397 pletely dissociating from their neighbors. Thus, our results support a mechanism in which
398 hybrid cells can maintain some functional characteristics of epithelial cells such as cell-
399 cell adhesion, which are normally lost in a fully differentiated mesenchymal state. The
400 tumor microenvironment contains many soluble signals simultaneously, including VEGF
401 and TGF- β . Thus, it is likely that some cancerous epithelial cells could exhibit hybrid EMT
402 phenotypic states. This may explain why fibroblastoid morphology, a classical feature of
403 EMT, is not commonly observed in human carcinomas (Debnath & Brugge, 2005). This
404 study focused on the combinatorial effects of two very different ligand families present to-

405 gether in the tumor environment. Additional modeling studies are required to unravel the
406 global response of epithelial cells to the full spectrum of chemical, substrate, and mechan-
407 ical cues. The simulation strategy presented here is readily adaptable to larger species
408 sets, with the major advantage that experimentally testable hypotheses can be generated
409 regarding how signals get integrated to produce global cellular response. Furthermore, by
410 simulating multiple ensembles of parameter sets, subpopulations across a constellation of
411 phenotypes can be created and mined for common and/or divergent signaling character-
412 istics. This is a significant advantage over forced convergence to a single unique solution
413 and thereby generating a potentially non-physiological homogeneous population.

414 The deterministic population of EMT models predicted heterogeneous behavior that
415 was qualitatively consistent with experimental studies. There is a diversity of algorithmic
416 approaches to estimate model parameters (Moles *et al.*, 2003), as well as many strategies
417 to integrate model identification with experimental design (Rodriguez-Fernandez *et al.*,
418 2013, Villaverde & Banga, 2014). However, despite these advances, the identification of
419 models describing intracellular network behavior remains challenging. There are differ-
420 ent schools of thought to deal with this challenge. One school has focused on model
421 reduction. Data-driven approaches (Cirit & Haugh, 2012), boolean (Choi *et al.*, 2012) or
422 other logical model formulations (Morris *et al.*, 2011, Terfve *et al.*, 2012) are emerging
423 paradigms that constrain model complexity by the availability of the training and validation
424 data. Other techniques such as constraints based modeling, which is commonly used
425 to model metabolic networks, have also been applied to model transcriptional networks,
426 although primarily in lower eukaryotes and prokaryotes (Hyduke & Palsson, 2010). These
427 techniques (and many others, see review (Wayman & Varner, 2013)) are certainly excit-
428 ing, with many interesting properties. Here, we used a traditional approach of mass action
429 kinetics within an ordinary differential equation framework that also included transfer func-
430 tions to simplify scenarios where reactions involving one species are controlled by several
431 others (e.g. E-cadherin transcription). The identification problem for the EMT model was

underdetermined (not uncommon for differential equation based models). However, a central criticism leveled by biologists is that model simplification is often done at the cost of biological reality, or done for reasons of computational expediency (Sainani, 2012). To avoid this criticism, we systematically identified an ensemble of likely models each consistent with the training data, instead of a single but uncertain best fit model. Previously, we (and others) have suggested that deterministic ensembles could model heterogeneous populations in situations where stochastic computation was not feasible (Lequieu *et al.*, 2011). Population heterogeneity using deterministic model families has previously been explored for bacterial growth in batch cultures (Lee *et al.*, 2009). In that case, distributions were generated because the model parameters varied over the ensemble, i.e., extrinsic noise led to population heterogeneity. In this study, parameters controlling physical interactions such as disassociation rates, or processes such as gene expression were distributed over the ensemble. Population heterogeneity can also arise from intrinsic thermal fluctuations, which are not captured by a deterministic population of models (Swain *et al.*, 2002). Thus, deterministic ensembles, provide a coarse-grained or extrinsic-only ability to simulate population diversity. Despite this limitation, our prediction of phenotypic heterogeneity (and the underlying signaling events responsible for the heterogeneity) was consistent with experimental observations. This suggested that deterministic ensembles could simulate disease or developmental processes in which heterogeneity plays an important role, without having to resort to stochastic simulation.

A common criticism of ODE modeling has been the poorly characterized effect of structural and parametric uncertainty. In this study, parametric uncertainty was addressed by developing an ensemble of probable models instead of a single best-fit but uncertain model using multiobjective optimization. While computationally complex, multiobjective optimization is an important tool to address qualitative conflicts in training data that arise from experimental error or cell line artifacts (Handl *et al.*, 2007). On the other hand, structural uncertainty is defined as uncertainty in the biological connectivity. The EMT model

459 connectivity was assembled from an extensive literature review. However, several poten-
460 tially important signaling mechanisms were not included. First, we identified a potential
461 gap in biological knowledge surrounding the regulation of LEF-1 expression, that was filled
462 by the addition of the hypothetical YREG1 transcriptional repressor. The LEF-1 transcrip-
463 tion factor is expressed in tissues that undergo EMT during embryogenesis (Nawshad &
464 Hay, 2003, Vega *et al.*, 2004), and has been suggested to promote an invasive phenotype
465 in cancer cells (Cano *et al.*, 2000, Kim *et al.*, 2002). Low levels of YREG1 were important
466 for stabilizing the interaction between LEF-1 and β -catenin, while elevated levels inhibited
467 EMT by downregulating LEF-1 transcriptional activity. Recent evidence has established a
468 complex role of Amino terminal Enhancer of Split (AES) and Groucho/TLE on suppress-
469 ing LEF-1 activity. AES opposes LEF-1 transcriptional activation while Groucho/TLE binds
470 with LEF-1 for a histone deacetylase repression. In addition, β -catenin directly displaces
471 Groucho/TLE repressors from TCF/LEF-1 in Wnt-mediated transcription activation (Arce
472 *et al.*, 2009, Grumolato *et al.*, 2013). Our model agrees with this newly discovered feed-
473 back system, as YREG1 regulates LEF-1 activity leading to EMT stabilization.

474 NF- κ B may also play an essential role of in the epithelial transformation. NF- κ B may
475 influence Snail expression through the AKT pathway and directly stabilize Snail activity
476 (Wu *et al.*, 2009). This is particularly important for integrating inflammation pathways,
477 such as interleukin-6 (IL-6) and tumor necrosis factor- α (TNF- α), which have been linked
478 to EMT in pathological conditions (Sullivan *et al.*, 2009). Other pathways such as Notch
479 have also been shown to act synergistically with TGF- β to express Slug in the developing
480 embryo (Niessen *et al.*, 2008). Lastly, while we have modeled classical protein signaling,
481 we have not considered the role of regulatory RNAs on EMT. There is growing evidence
482 that microRNAs (miRNAs) play a strong role in EMT, where several miRNAs, for example
483 miR-21 and miR-31 are strongly associated with TGF- β exposure (Bullock *et al.*, 2012).
484 Addressing missing structural components like these, could generate more insight into
485 TGF- β signaling and its role in phenotypic transformation.

486 **Materials and Methods**

487 The model code and parameter ensemble is freely available under an MIT software li-
488 cense and can be downloaded from <http://www.varnerlab.org>.

489 **Signaling network connectivity** The EMT model described the gene expression pro-
490 gram resulting from TGF- β and VEGF-A signaling in a prototypical epithelial cell. The
491 TGF- β -EMT network contained 97 nodes (proteins, mRNA or genes) interconnected by
492 251 interactions. The network connectivity was curated from more than 40 primary liter-
493 ature sources in combination with on-line databases (Jensen *et al.*, 2009, Linding *et al.*,
494 2007). The model interactome was not specific to a single epithelial cell line. Rather, we
495 assembled canonical pathways involved in TGF- β and VEGF-A signaling, defaulting to
496 human connectivity when possible. Using a canonical architecture allowed us to explore
497 general features of TGF- β induced EMT without cell line specific artifacts.

498 Our signaling network reconstruction was based on Medici *et al.* who identified the
499 pathways through which MDCKII, DLD1 colon carcinoma, and A375 melanoma cells tran-
500 sition towards a mesenchymal phenotype (Medici *et al.*, 2008). Sequential activation of
501 MAPK and Smad pathways were initiated upon addition of TGF- β 1/2. Briefly, TGF- β 2
502 signals through the RAS-RAF-MEK-ERK pathway to up-regulate Snail and Slug expres-
503 sion (Medici *et al.*, 2006). Snail, a known repressor of junctional proteins, inhibits the ex-
504 pression of E-cadherin (Cano *et al.*, 2000). This initial repression of E-cadherin leads to a
505 release of β -catenin from the cell membrane. This release of β -catenin can then translo-
506 cate to the nucleus and form transcriptional complexes with TCF-4 to drive TGF- β 3 ex-
507 pression (Medici *et al.*, 2008). The PI3K to GSK3 pathway was included and acted as
508 an activating mechanism of β -catenin signaling through TGF- β 3 signaling (Medici *et al.*,
509 2008). GSK3 is known to act on β -catenin signaling through the ubiquitin-proteasome
510 pathway (Larue & Bellacosa, 2005, Zhou *et al.*, 2004). Thereby, further β -catenin release
511 also resulted from by TGF- β 3 signals to the cells interior by binding to type II receptors,
512 which form heterodimers with type I receptors (ALK5) (Derynck & Zhang, 2003). This

activates the receptors serine/threonine kinase activity to phosphorylate and activate the receptor Smads 2/3 (Massagué *et al.*, 2005). In the model, receptors are simplified and represented as either bound or unbound complexes with their ligands. Phosphorylated Smads 2/3 (pSmad2/3) form heterodimers and translocate to the nucleus. pSmads complexes up-regulate other transcription factors, such as LEF-1. The pSmad2/4-LEF-1 complex has been shown to directly repress the E-cadherin gene (Nawshad *et al.*, 2007). LEF-1 also binds with β -catenin to upregulate mesenchymal proteins such as fibronectin (Medici *et al.*, 2011). In the model, Smad signaling is consolidated into a single Smad species that can act in a co-dependent fashion with LEF1 to downregulate E-cadherin via a transfer function, eliminating the need for an explicity LEF-1, pSmad complex. The EMT gene expression program was initiated by the binding of TGF- β isoforms to TGF- β surface receptors, starting the downstream signaling program. Repression of E-cadherin expression is the central event in the transition from an epithelial to a mesenchymal phenotype (Cano *et al.*, 2000). However, this transition is not solely driven by transcriptional events. At the protein level, the repression of E-cadherin leads to a release of β -catenin from cell membrane. Cytosolic β -catenin then translocates to the nucleus and forms transcriptionally-active complexes with immunoglobulin transcription factor 2 (TCF-4) to drive TGF- β 3 expression (Medici *et al.*, 2008). The PI3K to GSK3 pathway was included and acted as an activating mechanism of β -catenin signaling through TGF- β 3 signaling (Medici *et al.*, 2008). GSK3 is known to act on β -catenin signaling through APC complex associated ubiquitin-proteasome pathway. The APC complex is represented in our model and serves as a second reservoir of β -cateinin in untransformed cells whose sequestration is regulated by GSK3 (Larue & Bellacosa, 2005, Medici *et al.*, 2008, Zhou *et al.*, 2004). Lastly, VEGF-A activation of NFATc1 takes place through calcineurin signaling leading to an enhancement of E-cadherin expression (Suehiro *et al.*, 2014), as supported by our VEGF-A experimental data (Fig. S4).

Formulation, solution and analysis of the EMT model equations

540 *EMT signaling events.* EMT signaling events were modeled using either saturation or
 541 mass-action kinetics within an ordinary differential equation (ODE) framework:

$$\frac{1}{\tau_i} \frac{dx_i}{dt} = \sum_{j=1}^{\mathcal{R}} \sigma_{ij} r_j(\mathbf{x}, \epsilon, \mathbf{k}) - \mu x_i \quad i = 1, 2, \dots, \mathcal{M} \quad (1)$$

542 where \mathcal{R} denotes the number of signaling reactions and \mathcal{M} denotes the number of sig-
 543 naling proteins in the model. The quantity τ_i denotes a time scale parameter for species i
 544 which captures un-modeled effects; in the current study $\tau_i = 1$ for all species. The quan-
 545 tity $r_j(\mathbf{x}, \epsilon, \mathbf{k})$ denotes the rate of reaction j . Typically, reaction j is a non-linear function
 546 of biochemical and enzyme species abundance, as well as unknown model parameters \mathbf{k}
 547 ($\mathcal{K} \times 1$). The quantity σ_{ij} denotes the stoichiometric coefficient for species i in reaction j . If
 548 $\sigma_{ij} > 0$, species i is produced by reaction j . Conversely, if $\sigma_{ij} < 0$, species i is consumed
 549 by reaction j , while $\sigma_{ij} = 0$ indicates species i is not connected with reaction j . Species
 550 balances were subject to the initial conditions $\mathbf{x}(t_o) = \mathbf{x}_o$.

551 Rate processes were written as the product of a kinetic term (\bar{r}_j) and a control term (v_j)
 552 in the EMT model. The rate of enzyme catalyzed reactions was modeled using saturation
 553 kinetics:

$$\bar{r}_j = k_j^{cat} \epsilon_i \left(\frac{x_s}{K_{js} + x_s} \right) \quad (2)$$

554 where k_j^{cat} denotes the catalytic rate constant for reaction j , ϵ_i denotes the abundance of
 555 the enzyme catalyzing reaction j , and K_{js} denotes the saturation constant for species s
 556 in reaction j . On the other hand, mass action kinetics were used to model protein-protein
 557 binding interactions within the network:

$$\bar{r}_j = k_j^{max} \prod_{s \in m_j^-} x_s^{-\sigma_{sj}} \quad (3)$$

558 where k_j^{max} denotes the maximum rate for reaction j , σ_{sj} denotes the stoichiometric coef-
 559 ficient for species s in reaction j , and $s \in m_j$ denotes the set of *reactants* for reaction j .

560 Reversible binding was decomposed into two irreversible steps.

561 The control terms $0 \leq v_j \leq 1$ depended upon the combination of factors which in-
562 fluenced rate process j . For each rate, we used a rule-based approach to select from
563 competing control factors. If rate j was influenced by $1, \dots, m$ factors, we modeled this
564 relationship as $v_j = \mathcal{I}_j(f_{1j}(\cdot), \dots, f_{mj}(\cdot))$ where $0 \leq f_{ij}(\cdot) \leq 1$ denotes a regulatory
565 transfer function quantifying the influence of factor i on rate j . The function $\mathcal{I}_j(\cdot)$ is an
566 integration rule which maps the output of regulatory transfer functions into a control vari-
567 able. In this study, we used $\mathcal{I}_j \in \{\min, \max\}$ and hill transfer functions (Sagar & Varner,
568 2015, Wayman *et al.*, 2015). If a process has no modifying factors, $v_j = 1$.

569 *EMT gene expression processes.* The EMT model described both signal transduction
570 and gene expression events following the addition of TGF- β and VEGF-A. For each gene
571 of the $\mathcal{G} = 23$ we considered, we modeled both the resulting mRNA (m_j) and protein (p_j):

$$\frac{dm_j}{dt} = r_{T,j} - (\mu + \delta_{m,j}) m_j + \lambda_j \quad (4)$$

$$\frac{dp_j}{dt} = r_{X,j} - (\mu + \delta_{p,j}) p_j \quad (5)$$

572 where $j = 1, 2, \dots, \mathcal{G}$. The terms $r_{T,j}$ and $r_{X,j}$ denote the specific rates of transcription,
573 and translation while the terms $\delta_{m,j}$ and $\delta_{p,j}$ denote degradation constants for mRNA and
574 protein, respectively. Lastly, μ denotes the specific growth rate, and λ_j denotes the con-
575 stitutive rate of gene expression for gene j . The specific transcription rate was modeled
576 as the product of a kinetic term $\bar{r}_{T,j}$ and a control term u_j which described how the abun-
577 dance of transcription factors, or other regulators influenced the expression of gene j .

578 The kinetic rate of transcription was modeled as:

$$\bar{r}_{T,j} = \alpha_j \left[V_T^{\max} \left(\frac{G_j}{K_T + G_j} \right) \right] \quad (6)$$

579 where the maximum gene expression rate was defined as the product of a character-
580 istic transcription rate constant (k_T) and the abundance of RNA polymerase, $V_T^{\max} =$

581 k_T (*RNAP*). The parameter α_j denotes the gene specific correction to the characteris-
 582 tic transcription rate. (estimated in this study), while k_T , G_j and *RNAP* were estimated
 583 from literature (Milo *et al.*, 2010). Similar to the signaling processes, the gene expres-
 584 sion control term $0 \leq u_j \leq 1$ depended upon the combination of factors which influenced
 585 rate process j . For each rate, we used a rule-based approach to select from compet-
 586 ing control factors. If the expression of gene j was influenced by $1, \dots, m$ factors, we
 587 modeled this relationship as $u_j = \mathcal{I}_j(f_{1j}(\cdot), \dots, f_{mj}(\cdot))$ where $0 \leq f_{ij}(\cdot) \leq 1$ denotes a
 588 regulatory transfer function quantifying the influence of factor i on the expression of gene
 589 j . The function $\mathcal{I}_j(\cdot)$ is an integration rule which maps the output of regulatory transfer
 590 functions into a control variable. In this study, we used $\mathcal{I}_j \in \{\min, \max\}$ and hill transfer
 591 functions (Sagar & Varner, 2015, Wayman *et al.*, 2015). If a gene expression process has
 592 no modifying factors, $u_j = 1$. Lastly, the specific translation rate was modeled as:

$$r_{X,j} = \beta_j \left[V_X^{\max} \left(\frac{m_j}{K_X + m_j} \right) \right] \quad (7)$$

593 where V_X^{\max} denotes a characteristic maximum translation rate estimated from literature,
 594 β_j denotes the transcript specific correction the characteristic translation rate, and K_X
 595 denotes a translation saturation constant. The characteristic maximum translation rate
 596 was defined as the product of a characteristic translation rate constant (k_X) and the abun-
 597 dance of Ribosomes (*RIBO*), $V_X^{\max} = k_X (\text{RIBO})$, where both k_X and *RIBO* abundance
 598 were estimated from literature (Milo *et al.*, 2010).

599 In this study, we estimated k_T , k_X , *RNAP* and *RIBO* from literature. We calculated
 600 the concentration for gene j by assuming, on average, the cell had two copies of each
 601 gene at any given time. We also estimated characteristic values for $\delta_{m,j}$ and $\delta_{p,j}$, and
 602 corrected these values with mRNA/protein specific correction factors. Thus, the bulk of our
 603 gene expression parameters were based directly upon literature values. The values used
 604 for the characteristic transcription/translation parameters are given in the supplemental
 605 materials.

606 The signaling and gene expression model equations were implemented in Julia and
607 solved using the CVODE routine of the Sundials package (Bezanson *et al.*, 2014, Hindmarsh
608 *et al.*, 2005). The model code and parameter ensemble is freely available under an MIT
609 software license and can be downloaded from <http://www.varnerlab.org>.

610 *Estimation of model parameters using multiobjective optimization.* The EMT model had
611 296 unknown parameters (169 kinetic constants, 44 saturation constants, 38 control logic
612 parameters, and 45 non-zero initial conditions) which were not uniquely identifiable given
613 the training data. Instead, we estimated a population of likely models (each consistent
614 with the training data) using 41 data sets generated in DLD1 colon carcinoma, MDCKII,
615 and A375 melanoma cells taken from Medici *et al.* (Medici *et al.*, 2008). We used the
616 Pareto Optimal Ensemble Technique (JuPOETs) multiobjective optimization framework in
617 combination with leave-one-out cross-validation to estimate an ensemble of model pa-
618 rameters (Bassen *et al.*, 2016, Song *et al.*, 2010). Model parameter values were adjusted
619 to minimize the residual between simulations and experimental measurements for the 11
620 objective functions (supplemental materials). Cross-validation was used to calculate both
621 training and prediction error during the parameter estimation procedure (Kohavi, 1995).
622 The 41 intracellular protein and mRNA data-sets used for identification were organized
623 into 11 objective functions. These 11 objective functions were then partitioned, where
624 each partition contained ten training objectives and one validation objective. The training
625 and validation data were Western blots. We achieved a biologically realistic concentration
626 scale by establishing characteristic rates of transcription, translation, mRNA and protein
627 degradation, as well as characteristic concentrations of ribosomes and RNAPs using the
628 Bionumbers database (Milo *et al.*, 2010), (supplemental materials). The overall concen-
629 tration scale was nM, with proteins ranging from 10-1000nM and mRNA ranging from 0.01
630 to 1nM, reflecting the true abundances and ratios between each species. An initial nom-
631 inal parameter set was established by inspection. JuPOETs was then allowed to search
632 in a neighborhood of $\pm 30\%$ of this nominal set. The parameter ensemble estimated by

633 JuPOETs is available with the model source code. JuPOETs is open source and freely
634 available for download under an MIT software license from <http://www.varnerlab.org>.

635 **Cell culture and experimental interrogation** DLD1 colon carcinoma, MCF10A, and
636 HUVEC were acquired from the American Tissue Culture Collection (Manassas, VA).
637 Cells were grown in culture with RPMI 1640 medium with 10% fetal bovine serum and
638 1% penicillin/streptomycin for DLD1, EBM-2 supplemented with EGM-2, 5% fetal bovine
639 serum, and 1% penicillin/streptomycin for HUVEC, or MGEM 2 supplemented with insulin,
640 bovine pituitary extract, cholera toxin, hEGF, hydrocortisone, 5% horse serum, and 1%
641 penicillin/streptomycin for MCF10A. Cells were serum starved for 24 hours and removed
642 from all experimental conditions. Recombinant VEGFA165 was also removed from cul-
643 ture medium prior to experimentation. Recombinant human TGF- β 2 (R & D Systems,
644 Minneapolis, MN) was added to the culture medium at a concentration of 10 ng/ml and re-
645 combinant VEGFA165 at a concentration of (5ng/ml, 50ng/ml) for all relative experiments.
646 NFAT inhibitor (VIVIT peptide) (EMDBiosciences, Darmstadt, Germany), was added to
647 the culture medium at a concentration of 10 μ M for all relative experiments. Cells were
648 passaged 1:3 or 1:4 every 3-6 d and used between passages 4 and 8.

649 *VEGF treatment* DLD1 and MCF10A cells were suspended in culture media (with RPMI
650 1640 medium with 10% fetal bovine serum and 1% penicillin/streptomycin for DLD1 or
651 MGEM 2 supplemented with insulin, bovine pituitary extract, cholera toxin, hEGF, hydro-
652 cortisone, 5% horse serum, and 1% penicillin/streptomycin for MCF10A), and allowed to
653 aggregate overnight in hanging drop culture (20 μ L; 20,000 cells). The spherical aggre-
654 gates were placed on the surface of neutralized type I collagen hydrogels (1.5mg/mL)
655 and allowed to adhere. Cultures were then serum starved (1% serum) for 24 hours. Re-
656 combinant VEGFA165 was then added to the media (5ng/ml, 50ng/ml) and mRNA was
657 harvested after 3hr and 24hr timepoint.

658 *RT-PCR* RNA extractions were performed using a Qiagen total RNA purification kit (Qi-
659 agen, Valencia, CA) and RNA was reverse transcribed to cDNA using the SuperScript

660 III RT-PCR kit with oligo(dT) primer (Invitrogen). Sufficient quality RNA was determined
661 by an absorbance ratio A260/A280 of 1.8-2.1, while the quantity of RNA was determined
662 by measuring the absorbance at 260nm (A260). Real-time PCR experiments were con-
663 ducted using the SYBR Green PCR system (Biorad, Hercules, CA) on a Biorad CFX96
664 cycler, with 40 cycles per sample. Cycling temperatures were as follows: denaturing,
665 95C; annealing, 60C; and extension, 70C. Primers were designed to detect GAPDH, E-
666 cadherin, vimentin, Slug, Sp1, and NFATc1 in cDNA clones: Sp1 (F-TTG AAA AAG GAG
667 TTG GTG GC, R-TGC TGG TTC TGT AAG TTG GG, Accession NG030361.1), NFATc1
668 (F-GCA TCA CAG GGA AGA CCG TGT C, R-GAA GTT CAA TGT CGG AGT TTC TGA
669 G, Accession NG029226.1). GAPDH, E-cadherin, vimentin, and Slug primers were taken
670 from previously published literature (Medici *et al.*, 2008).

671 *Antibody Staining* Samples were fixed in 4% PFA overnight at 4C. Samples were then
672 washed for 15 minutes on a rocker 3 times with PBS, permeabilized with 0.2% Triton-X
673 100 (VWR International, Radnor, PA) for 10 minutes, and washed another 3 times with
674 PBS. Samples were incubated overnight at 4C in a 1% BSA (Rockland Immunochemi-
675 cals, Inc., Gilbertsville, PA) blocking solution followed by another 4C overnight incubation
676 with either rabbit anti-human E-cadherin 1:100 (Abcam, ab53033), mouse anti-human
677 phospho-Sp1 1:100 (Abcam, ab37707), mouse anti-human vimentin 1:100 (Invitrogen,
678 V9), and rabbit anti-human NFATc1 (Santa Cruz, sc-7294) 1:100. After 3 washes for 15
679 minutes with PBS, samples were exposed to Alexa Fluor 488 or 568 conjugated (Invit-
680 rogen), species specific secondary antibodies at 1:100 in 1% BSA for 2 hours at room
681 temperature. Three more washes with PBS for 15 minutes were followed by incubation
682 with either DRAQ5 far red nuclear stain (Enzo Life Sciences, Plymouth Meeting, PA) at
683 1:1000.

684 *FACS* Flow cytometry for E-cadherin 1:100 (Abcam) and vimentin 1:100 expressing cells
685 was performed. Briefly, cells were trypsinized, fixed with 4% PFA for 10 min and then pre-
686 served in 50% methanol/PBS. Cells were kept in the -20C until antibody staining was

687 preformed. Samples were divided into multiple aliquots in order to stain the proteins
688 separately and compensate for secondary antibody non-specific binding. Cells were in-
689 cubated for 24 hrs at 4 C in primary antibody diluted in either PBS (extracellular) or 0.2%
690 saponin-PBS (intracellular). Cells were then washed 3 times with PBS and incubated
691 with appropriate secondary antibodies and imaged using a Coulter Epics XL-MCL Flow
692 Cytometer (Coulter). All samples were compensated using appropriate background sub-
693 traction and all samples were normalized using 7500 cells per flow condition.

694 *Three-Dimensional Culture and Tubulogenesis Assays* For invasion/migration assays,
695 cells were resuspended in culture media, and allowed to aggregate overnight in hanging
696 drop culture ($20\mu\text{L}$; 20,000 cells). The spherical aggregates were placed on the surface of
697 neutralized type I collagen hydrogels (1.5mg/mL) and allowed to adhere for 2 hrs before
698 adding treatments. Cultures were maintained for 72 hrs, after which they were fixed in
699 4% PFA and slowly rehydrated using PBS. For compaction assays, cells were pelleted
700 via centrifugation and resuspended within a neutralized collagen hydrogel (1.5mg/mL)
701 solution at a density of 400,000 cells/mL. $250\mu\text{L}$ of gel was inoculated into culture wells,
702 which solidified after 60min. Treatments were then added within $800\mu\text{L}$ of the culture
703 medium without serum. Gels were liberated from the surfaces of the culture wells the
704 next day and cultured free floating for an additional 3-7 days, exchanging serum free
705 media with appropriate factors every 48 hrs.

706 Tubulogenesis was defined as a typical nonmalignant acini structure. This includes a
707 polarized epithelial cell, hollow lumen, and the basal sides of the cell are surrounded by
708 ECM proteins (Fig. 6A, Controls or VEGF treated). Previous work has shown that change
709 in the morphological characteristics of nontumorigenic MCF10A epithelial acini occur over
710 time and exploiting them to growth in 3D culture can be quantified. For example, using
711 image segmentation, Chang et al. (Chang *et al.*, 2007) examined the elongation of the
712 MCF10A acini at 6, 12, and 96 hours after a particular treatment. Polizzotti et al. (Poliz-
713 zotti *et al.*, 2012) also suggested a computational method to quantify acini structure based

⁷¹⁴ on morphological characteristics in nonmalignant, noninvasive, and invasive conditions.
⁷¹⁵ Adapted from these approaches, we first fluorescently labeled our cultures and captured
⁷¹⁶ the acini structures by 3D confocal microscopy. Next individual acini structures in the im-
⁷¹⁷ ages were segmented by imageJ and labeled. We then extracted the number of ductal
⁷¹⁸ branches. Ductal branching was defined as any elongated cell cluster extending away
⁷¹⁹ from the total acini structure, which was manually segmented and counted using ImageJ.
⁷²⁰ A total of 5 images for each condition were used, and approximately 12 acini were ana-
⁷²¹ lyzed in each image. Total branching was normalized to the amount of acini present, and
⁷²² provides an overall general assessment to the extent of acini remodeling.

⁷²³ *Statistics* Results are expressed as mean \pm standard error, $n \geq 6$. Data was analyzed
⁷²⁴ with the GraphPad Prism version 4.00 for Windows (GraphPad Software, San Diego,
⁷²⁵ CA) and SAS (Statistical Analysis Software, Cary, NC). A one-way ANOVA with Tukey's
⁷²⁶ post hoc was used to compare differences between means and data was transformed
⁷²⁷ when necessary to obtain equal sample variances. Differences between means were
⁷²⁸ considered significant at $p < 0.05$.

729 **References**

- 730 Abramoff M, Magelhaes P, Ram S (2004) Image Processing with ImageJ. *Biophotonics International*, **11**: 36–42
- 731 Ahmed S, Nawshad A (2007) Complexity in interpretation of embryonic epithelial-mesenchymal transition in response to transforming growth factor-beta signaling. *Cells Tissues Organs* **185**: 131–45
- 732 Aramburu J, Yaffe MB, López-Rodríguez C, Cantley LC, Hogan PG, Rao A (1999) Affinity-driven peptide selection of an NFAT inhibitor more selective than cyclosporin A. *Science* **285**: 2129–33
- 733 734 735 736 737 738 739 740 741 742 743 744 745 746 747 748 749 750 751 752 753 754 755 Arce L, Pate KT, Waterman ML (2009) Groucho binds two conserved regions of LEF-1 for HDAC-dependent repression. *BMC Cancer* **9**: 159
- Bailey JE (2001) Complex biology with no parameters. *Nat Biotechnol* **19**: 503–4
- Bassen D, Vilkovoy M, Minot M, Butcher JT, Varner JD (2016) JuPOETs: A Constrained Multiobjective Optimization Approach to Estimate Biochemical Model Ensembles in the Julia Programming Language. *bioRxiv* **10.1101/056044**
- Bezanson J, Edelman A, Karpinski S, Shah VB (2014) Julia: A Fresh Approach to Numerical Computing. *CoRR* **abs/1411.1607**
- Bullock MD, Sayan AE, Packham GK, Mirnezami AH (2012) MicroRNAs: critical regulators of epithelial to mesenchymal (EMT) and mesenchymal to epithelial transition (MET) in cancer progression. *Biol Cell* **104**: 3–12
- Butcher JT, Penrod AM, García AJ, Nerem RM (2004) Unique morphology and focal adhesion development of valvular endothelial cells in static and fluid flow environments. *Arterioscler Thromb Vasc Biol* **24**: 1429–34
- Cano A, Pérez-Moreno MA, Rodrigo I, Locascio A, Blanco MJ, del Barrio MG, Portillo F, Nieto MA (2000) The transcription factor snail controls epithelial-mesenchymal transitions by repressing E-cadherin expression. *Nat Cell Biol* **2**: 76–83
- Chang H, Park C, Parvin B (2007) Quantitative Representation of Three-dimensional Cell

- 756 Culture Models. In *Proceedings of the 2007 IEEE International Symposium on Biomed-*
757 *ical Imaging: From Nano to Macro, Washington, DC, USA, April 12-16, 2007*. pp. 89–92
- 758 Chen WW, Schoeberl B, Jasper PJ, Niepel M, Nielsen UB, Lauffenburger DA, Sorger PK
759 (2009) Input-output behavior of ErbB signaling pathways as revealed by a mass action
760 model trained against dynamic data. *Mol Syst Biol* **5**: 239
- 761 Choi M, Shi J, Jung SH, Chen X, Cho KH (2012) Attractor landscape analysis reveals
762 feedback loops in the p53 network that control the cellular response to DNA damage.
763 *Sci Signal* **5**: ra83
- 764 Chung SW, Miles FL, Sikes RA, Cooper CR, Farach-Carson MC, Ogunnaike BA (2009)
765 Quantitative modeling and analysis of the transforming growth factor beta signaling
766 pathway. *Biophys J* **96**: 1733–50
- 767 Cirit M, Haugh JM (2012) Data-driven modelling of receptor tyrosine kinase signalling
768 networks quantifies receptor-specific potencies of PI3K- and Ras-dependent ERK acti-
769 vation. *Biochem J* **441**: 77–85
- 770 Creixell P, Schoof EM, Erler JT, Linding R (2012) Navigating cancer network attractors for
771 tumor-specific therapy. *Nat Biotechnol* **30**: 842–8
- 772 Debnath J, Brugge JS (2005) Modelling glandular epithelial cancers in three-dimensional
773 cultures. *Nat Rev Cancer* **5**: 675–88
- 774 Debnath J, Muthuswamy SK, Brugge JS (2003) Morphogenesis and oncogenesis of MCF-
775 10A mammary epithelial acini grown in three-dimensional basement membrane cul-
776 tures. *Methods* **30**: 256–268
- 777 Deryck R, Zhang YE (2003) Smad-dependent and Smad-independent pathways in TGF-
778 beta family signalling. *Nature* **425**: 577–84
- 779 Dhasarathy A, Phadke D, Mav D, Shah RR, Wade PA (2011) The transcription factors
780 Snail and Slug activate the transforming growth factor-beta signaling pathway in breast
781 cancer. *PLoS One* **6**: e26514
- 782 Dhimolea E, Maffini MV, Soto AM, Sonnenschein C (2010) The role of collagen reorgani-

- 783 zation on mammary epithelial morphogenesis in a 3D culture model. *Biomaterials* **31**:
784 3622–3630
- 785 Eastman Q, Grosschedl R (1999) Regulation of LEF-1/TCF transcription factors by Wnt
786 and other signals. *Curr Opin Cell Biol* **11**: 233–40
- 787 Eisenberg LM, Markwald RR (1995) Molecular regulation of atrioventricular valvuloseptal
788 morphogenesis. *Circ Res* **77**: 1–6
- 789 Ferrara N (2002) VEGF and the quest for tumour angiogenesis factors. *Nat Rev Cancer*
790 **2**: 795–803
- 791 Gadkar KG, Varner J, Doyle FJ 3rd (2005) Model identification of signal transduction
792 networks from data using a state regulator problem. *Syst Biol (Stevenage)* **2**: 17–30
- 793 Grumolato L, Liu G, Haremaiki T, Mungamuri SK, Mong P, Akiri G, Lopez-Bergami P, Arita
794 A, Anouar Y, Mlodzik M, Ronai ZA, Brody J, Weinstein DC, Aaronson SA (2013) ?-
795 Catenin-Independent Activation of TCF1/LEF1 in Human Hematopoietic Tumor Cells
796 through Interaction with ATF2 Transcription Factors. *PLoS Genet* **9**: e1003603
- 797 Guaita S, Puig I, Franci C, Garrido M, Dominguez D, Batlle E, Sancho E, Dedhar S,
798 De Herreros AG, Baulida J (2002) Snail induction of epithelial to mesenchymal transition
799 in tumor cells is accompanied by MUC1 repression and ZEB1 expression. *J Biol Chem*
800 **277**: 39209–16
- 801 Handl J, Kell DB, Knowles J (2007) Multiobjective optimization in bioinformatics and com-
802 putational biology. *IEEE/ACM Trans Comput Biol Bioinform* **4**: 279–92
- 803 Hardy KM, Booth BW, Hendrix MJC, Salomon DS, Strizzi L (2010) ErbB/EGF signaling
804 and EMT in mammary development and breast cancer. *J Mammary Gland Biol Neo-*
805 *plasia* **15**: 191–9
- 806 Hasenauer J, Waldherr S, Doszczak M, Radde N, Scheurich P, Allgöwer F (2011) Iden-
807 tification of models of heterogeneous cell populations from population snapshot data.
808 *BMC Bioinformatics* **12**: 125
- 809 Hemavathy K, Ashraf SI, Ip YT (2000a) Snail/slug family of repressors: slowly going into

- 810 the fast lane of development and cancer. *Gene* **257**: 1–12
- 811 Hemavathy K, Guru SC, Harris J, Chen JD, Ip YT (2000b) Human Slug is a repressor that
812 localizes to sites of active transcription. *Mol Cell Biol* **20**: 5087–95
- 813 Hindmarsh A, Brown P, Grant K, Lee S, Serban R, Shumaker D, Woodward C (2005) SUN-
814 DIALS: Suite of nonlinear and differential/algebraic equation solvers. *ACM Transactions*
815 *on Mathematical Software* **31**: 363–396
- 816 Hong JP, Li XM, Li MX, Zheng FL (2013) VEGF suppresses epithelial-mesenchymal tran-
817 sition by inhibiting the expression of Smad3 and miR-192 a Smad3-dependent mi-
818 croRNA. *Int J Mol Med* **31**: 1436–42
- 819 Huber MA, Azoitei N, Baumann B, Grünert S, Sommer A, Pehamberger H, Kraut N, Beug
820 H, Wirth T (2004) NF-kappaB is essential for epithelial-mesenchymal transition and
821 metastasis in a model of breast cancer progression. *J Clin Invest* **114**: 569–81
- 822 Hyduke DR, Palsson BØ (2010) Towards genome-scale signalling network reconstruc-
823 tions. *Nat Rev Genet* **11**: 297–307
- 824 Jackstadt R, Röh S, Neumann J, Jung P, Hoffmann R, Horst D, Berens C, Bornkamm
825 GW, Kirchner T, Menssen A, Hermeking H (2013) AP4 is a mediator of epithelial-
826 mesenchymal transition and metastasis in colorectal cancer. *J Exp Med* **210**: 1331–50
- 827 Jensen LJ, Kuhn M, Stark M, Chaffron S, Creevey C, Muller J, Doerks T, Julien P, Roth
828 A, Simonovic M, Bork P, von Mering C (2009) STRING 8—a global view on proteins and
829 their functional interactions in 630 organisms. *Nucleic Acids Res* **37**: D412–6
- 830 Jiang YG, Luo Y, He DI, Li X, Zhang LI, Peng T, Li MC, Lin YH (2007) Role of Wnt/beta-
831 catenin signaling pathway in epithelial-mesenchymal transition of human prostate can-
832 cer induced by hypoxia-inducible factor-1alpha. *Int J Urol* **14**: 1034–9
- 833 Kalita MK, Sargsyan K, Tian B, Paulucci-Holthauzen A, Najm HN, Debusschere BJ,
834 Brasier AR (2011) Sources of cell-to-cell variability in canonical nuclear factor-kB (NF-
835 kB) signaling pathway inferred from single cell dynamic images. *J Biol Chem* **286**:
836 37741–57

- 837 Kim K, Lu Z, Hay ED (2002) Direct evidence for a role of beta-catenin/LEF-1 signaling
838 pathway in induction of EMT. *Cell Biol Int* **26**: 463–76
- 839 Kohavi R (1995) A study of cross-validation and bootstrap for accuracy estimation and
840 model selection. In *International joint Conference on artificial intelligence*, vol. 14. Cite-
841 seer, pp. 1137–1145
- 842 Larue L, Bellacosa A (2005) Epithelial-mesenchymal transition in development and can-
843 cer: role of phosphatidylinositol 3' kinase/AKT pathways. *Oncogene* **24**: 7443–54
- 844 Lee MW, Vassiliadis VS, Park JM (2009) Individual-based and stochastic modeling of cell
845 population dynamics considering substrate dependency. *Biotechnol Bioeng* **103**: 891–9
- 846 Lequieu J, Chakrabarti A, Nayak S, Varner JD (2011) Computational modeling and anal-
847 ysis of insulin induced eukaryotic translation initiation. *PLoS Comput Biol* **7**: e1002263
- 848 Lian Yg, Zhou Qg, Zhang Yj, Zheng Fl (2011) VEGF ameliorates tubulointerstitial fibrosis
849 in unilateral ureteral obstruction mice via inhibition of epithelial-mesenchymal transition.
850 *Acta Pharmacol Sin* **32**: 1513–21
- 851 Linding R, Jensen LJ, Osthimer GJ, van Vugt MATM, Jørgensen C, Miron IM, Diella F,
852 Colwill K, Taylor L, Elder K, Metalnikov P, Nguyen V, Pascalescu A, Jin J, Park JG, Sam-
853 son LD, Woodgett JR, Russell RB, Bork P, Yaffe MB, et al. (2007) Systematic discovery
854 of in vivo phosphorylation networks. *Cell* **129**: 1415–26
- 855 Luan D, Szlam F, Tanaka KA, Barie PS, Varner JD (2010) Ensembles of uncertain mathe-
856 matical models can identify network response to therapeutic interventions. *Mol Biosyst*
857 **6**: 2272–86
- 858 Machta BB, Chachra R, Transtrum MK, Sethna JP (2013) Parameter space compression
859 underlies emergent theories and predictive models. *Science* **342**: 604–7
- 860 Mancini M, Toker A (2009) NFAT proteins: emerging roles in cancer progression. *Nat Rev*
861 *Cancer* **9**: 810–820
- 862 Massagué J, Seoane J, Wotton D (2005) Smad transcription factors. *Genes Dev* **19**:
863 2783–810

- 864 Medici D, Hay ED, Goodenough DA (2006) Cooperation between snail and LEF-1 trans-
865cription factors is essential for TGF-beta1-induced epithelial-mesenchymal transition.
866 *Mol Biol Cell* **17**: 1871–9
- 867 Medici D, Hay ED, Olsen BR (2008) Snail and Slug promote epithelial-mesenchymal tran-
868sition through beta-catenin-T-cell factor-4-dependent expression of transforming growth
869 factor-beta3. *Mol Biol Cell* **19**: 4875–87
- 870 Medici D, Potenta S, Kalluri R (2011) Transforming growth factor-?2 promotes
871 Snail-mediated endothelial-mesenchymal transition through convergence of Smad-
872 dependent and Smad-independent signalling. *Biochem J* **437**: 515–520
- 873 Milo R, Jorgensen P, Moran U, Weber G, Springer M (2010) BioNumbers—the database
874 of key numbers in molecular and cell biology. *Nucleic Acids Res* **38**: D750–3
- 875 Moles CG, Mendes P, Banga JR (2003) Parameter estimation in biochemical pathways: a
876 comparison of global optimization methods. *Genome Res* **13**: 2467–74
- 877 Morris MK, Saez-Rodriguez J, Clarke DC, Sorger PK, Lauffenburger DA (2011) Training
878 signaling pathway maps to biochemical data with constrained fuzzy logic: quantitative
879 analysis of liver cell responses to inflammatory stimuli. *PLoS Comput Biol* **7**: e1001099
- 880 Nagy JA, Dvorak AM, Dvorak HF (2007) VEGF-A and the induction of pathological angio-
881 genesis. *Annu Rev Pathol* **2**: 251–75
- 882 Nawshad A, Hay ED (2003) TGFbeta3 signaling activates transcription of the LEF1 gene
883 to induce epithelial mesenchymal transformation during mouse palate development. *J
884 Cell Biol* **163**: 1291–301
- 885 Nawshad A, Medici D, Liu CC, Hay ED (2007) TGFbeta3 inhibits E-cadherin gene expres-
886 sion in palate medial-edge epithelial cells through a Smad2-Smad4-LEF1 transcription
887 complex. *J Cell Sci* **120**: 1646–53
- 888 Neve RM, Chin K, Fridlyand J, Yeh J, Baehner FL, Fevr T, Clark L, Bayani N, Coppe JP,
889 Tong F, Speed T, Spellman PT, DeVries S, Lapuk A, Wang NJ, Kuo WL, Stilwell JL,
890 Pinkel D, Albertson DG, Waldman FM, *et al.* (2006) A collection of breast cancer cell

- 891 lines for the study of functionally distinct cancer subtypes. *Cancer Cell* **10**: 515–27
- 892 Niessen K, Fu Y, Chang L, Hoodless PA, McFadden D, Karsan A (2008) Slug is a direct
893 Notch target required for initiation of cardiac cushion cellularization. *J Cell Biol* **182**:
894 315–25
- 895 O'Brien LE, Tang K, Kats ES, Schutz-Geschwender A, Lipschutz JH, Mostov KE (2004)
896 ERK and MMPs sequentially regulate distinct stages of epithelial tubule development.
897 *Dev Cell* **7**: 21–32
- 898 Park SY, Lee HE, Li H, Shipitsin M, Gelman R, Polyak K (2010) Heterogeneity for stem
899 cell-related markers according to tumor subtype and histologic stage in breast cancer.
900 *Clin Cancer Res* **16**: 876–87
- 901 Pearson GW, Hunter T (2007) Real-time imaging reveals that noninvasive mammary ep-
902 ithelial acini can contain motile cells. *J Cell Biol* **179**: 1555–67
- 903 Polizzotti L, Basak O, Bjornsson C, Shubert K, Yener B, Plopper G (2012) Novel Image
904 Analysis Approach Quantifies Morphological Characteristics of 3D Breast Culture Acini
905 with Varying Metastatic Potentials. *J Biomed Biotech* **2012**: 1–16
- 906 Polyak K, Weinberg RA (2009) Transitions between epithelial and mesenchymal states:
907 acquisition of malignant and stem cell traits. *Nat Rev Cancer* **9**: 265–273
- 908 Rodriguez-Fernandez M, Rehberg M, Kremling A, Banga JR (2013) Simultaneous model
909 discrimination and parameter estimation in dynamic models of cellular systems. *BMC
910 Syst Biol* **7**: 76
- 911 Sagar A, Varner JD (2015) Dynamic Modeling of the Human Coagulation Cascade Using
912 Reduced Order Effective Kinetic Models. *Processes* **3**: 178
- 913 Sainani KL (2012) Meet the Skeptics: Why some doubt biomedical models - and what it
914 takes to win them over. *Biomedical Computation Review* : 12 – 18
- 915 Schoeberl B, Eichler-Jonsson C, Gilles ED, Muller G (2002) Computational modeling of
916 the dynamics of the MAP kinase cascade activated by surface and internalized EGF
917 receptors. *Nat Biotechnol* **20**: 370–375

- 918 Singh G, Singh SK, König A, Reutlinger K, Nye MD, Adhikary T, Eilers M, Gress TM,
919 Fernandez-Zapico ME, Ellenrieder V (2010) Sequential activation of NFAT and c-Myc
920 transcription factors mediates the TGF-beta switch from a suppressor to a promoter of
921 cancer cell proliferation. *J Biol Chem* **285**: 27241–50
- 922 Song SO, Chakrabarti A, Varner JD (2010) Ensembles of signal transduction models
923 using Pareto Optimal Ensemble Techniques (POETs). *Biotechnol J* **5**: 768–80
- 924 Stahl PJ, Felsen D (2001) Transforming growth factor-beta, basement membrane, and
925 epithelial-mesenchymal transdifferentiation: implications for fibrosis in kidney disease.
926 *Am J Pathol* **159**: 1187–92
- 927 Strauss R, Li ZY, Liu Y, Beyer I, Persson J, Sova P, Möller T, Pesonen S, Hemminki A,
928 Hamerlik P, Drescher C, Urban N, Bartek J, Lieber A (2011) Analysis of epithelial and
929 mesenchymal markers in ovarian cancer reveals phenotypic heterogeneity and plastic-
930 ity. *PLoS One* **6**: e16186
- 931 Suehiro Ji, Kanki Y, Makihara C, Schadler K, Miura M, Manabe Y, Aburatani H, Kodama
932 T, Minami T (2014) Genome-wide approaches reveal functional vascular endothelial
933 growth factor (VEGF)-inducible nuclear factor of activated T cells (NFAT) c1 binding to
934 angiogenesis-related genes in the endothelium. *J Biol Chem* **289**: 29044–59
- 935 Sullivan NJ, Sasser AK, Axel AE, Vesuna F, Raman V, Ramirez N, Oberyszyn TM, Hall BM
936 (2009) Interleukin-6 induces an epithelial-mesenchymal transition phenotype in human
937 breast cancer cells. *Oncogene* **28**: 2940–7
- 938 Swain PS, Elowitz MB, Siggia ED (2002) Intrinsic and extrinsic contributions to stochas-
939 ticity in gene expression. *Proc Natl Acad Sci U S A* **99**: 12795–800
- 940 Tasseff R, Nayak S, Song SO, Yen A, Varner JD (2011) Modeling and analysis of retinoic
941 acid induced differentiation of uncommitted precursor cells. *Integr Biol (Camb)* **3**: 578–
942 591
- 943 Terfve C, Cokelaer T, Henriques D, MacNamara A, Goncalves E, Morris MK, van Iersel M,
944 Lauffenburger DA, Saez-Rodriguez J (2012) CellNOptR: a flexible toolkit to train protein

- 945 signaling networks to data using multiple logic formalisms. *BMC Syst Biol* **6**: 133
- 946 Thiery JP (2003) Epithelial-mesenchymal transitions in development and pathologies.
- 947 *Curr Opin Cell Biol* **15**: 740–6
- 948 Vega S, Morales AV, Ocaña OH, Valdés F, Fabregat I, Nieto MA (2004) Snail blocks the
- 949 cell cycle and confers resistance to cell death. *Genes Dev* **18**: 1131–43
- 950 Vilar JMG, Jansen R, Sander C (2006) Signal processing in the TGF-beta superfamily
- 951 ligand-receptor network. *PLoS Comput Biol* **2**: e3
- 952 Villaverde AF, Banga JR (2014) Reverse engineering and identification in systems biology:
- 953 strategies, perspectives and challenges. *J R Soc Interface* **11**: 20130505
- 954 Wayman J, Varner J (2013) Biological systems modeling of metabolic and signaling net-
- 955 works. *Curr Opin Chem Eng* **2**: 365 – 372
- 956 Wayman JA, Sagar A, Varner JD (2015) Dynamic Modeling of Cell-Free Biochemical Net-
- 957 works Using Effective Kinetic Models. *Processes* **3**: 138
- 958 Welch-Reardon KM, Wu N, Hughes CCW (2014) A Role for Partial Endothelial-
- 959 Mesenchymal Transitions in Angiogenesis? *Arterioscler Thromb Vasc Biol*
- 960 Willis BC, Borok Z (2007) TGF-beta-induced EMT: mechanisms and implications for fi-
- 961 brotic lung disease. *Am J Physiol Lung Cell Mol Physiol* **293**: L525–34
- 962 Wu Y, Deng J, Rychahou PG, Qiu S, Evers BM, Zhou BP (2009) Stabilization of snail by
- 963 NF-kappaB is required for inflammation-induced cell migration and invasion. *Cancer*
- 964 *Cell* **15**: 416–28
- 965 Xu J, Lamouille S, Derynck R (2009) TGF-beta-induced epithelial to mesenchymal transi-
- 966 tion. *Cell Res* **19**: 156–72
- 967 Zajchowski DA, Bartholdi MF, Gong Y, Webster L, Liu HL, Munishkin A, Beauheim C,
- 968 Harvey S, Ethier SP, Johnson PH (2001) Identification of gene expression profiles that
- 969 predict the aggressive behavior of breast cancer cells. *Cancer Res* **61**: 5168–78
- 970 Zavadil J, Böttlinger EP (2005) TGF-beta and epithelial-to-mesenchymal transitions.
- 971 *Oncogene* **24**: 5764–74

⁹⁷² Zhou BP, Deng J, Xia W, Xu J, Li YM, Gunduz M, Hung MC (2004) Dual regulation of Snail
⁹⁷³ by GSK-3beta-mediated phosphorylation in control of epithelial-mesenchymal transi-
⁹⁷⁴ tion. *Nat Cell Biol* **6**: 931–40

Extracellular

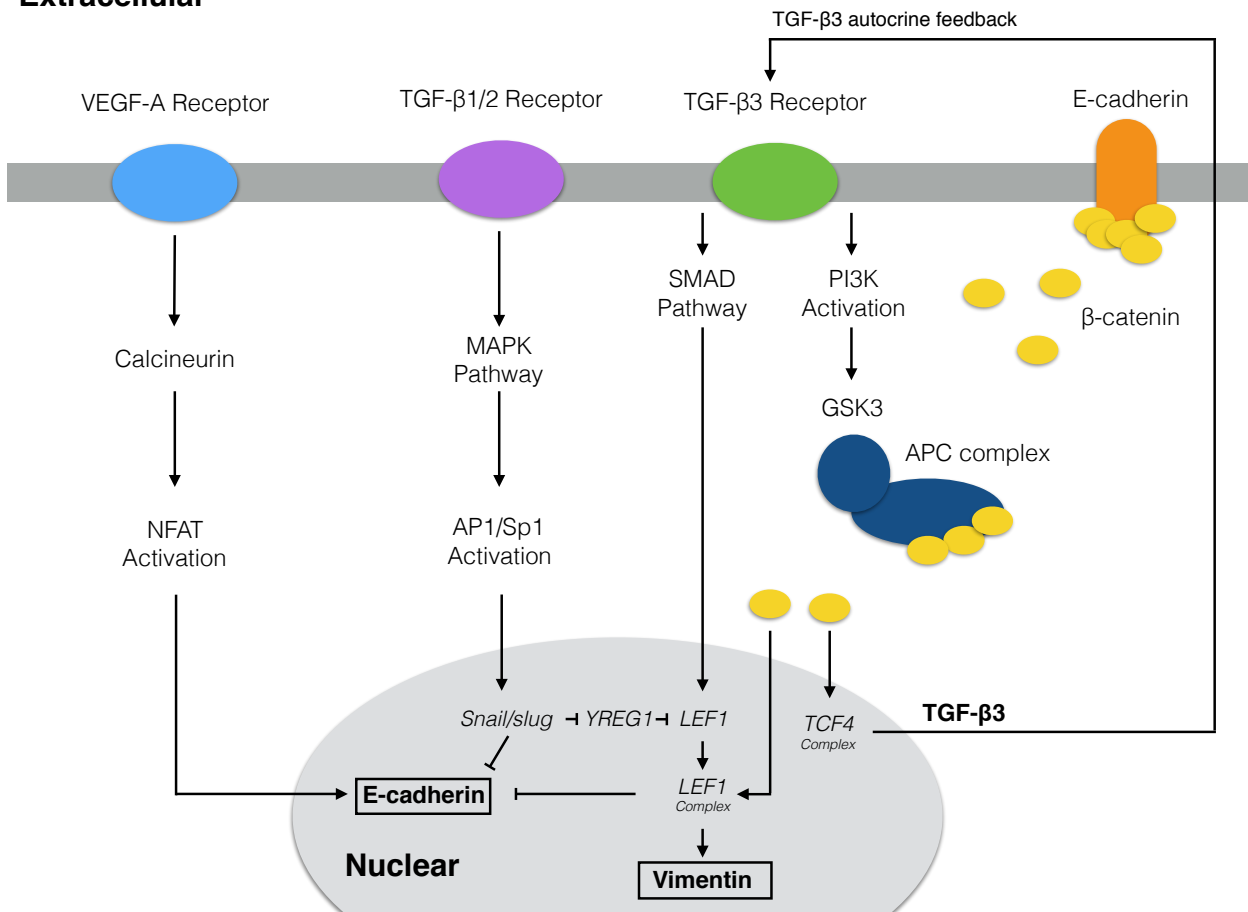


Fig. 1: Model connectivity recreates the core architecture during EMT. The EMT network contains 97 nodes (proteins, mRNA, and genes) interconnected by 169 interactions. Central to EMT induction, activation of the MAPK cascade occurs through TGF- β 1/2 binding which activates the AP-1/Sp1 transcriptional axis. AP-1/Sp1 drives an autocrine response of TGF- β 3, which activates the Smad cascade, leading to phenotypic change. Conversely, VEGF-A binding can stabilize an epithelial phenotype through NFAT activation. Downstream activation of β -catenin signaling due to E-cadherin loss and GSK3 inactivation of β -catein in confinement is critical to the complete activation of the EMT program. The complete list of molecular interactions that comprise the model is given in the supplement.

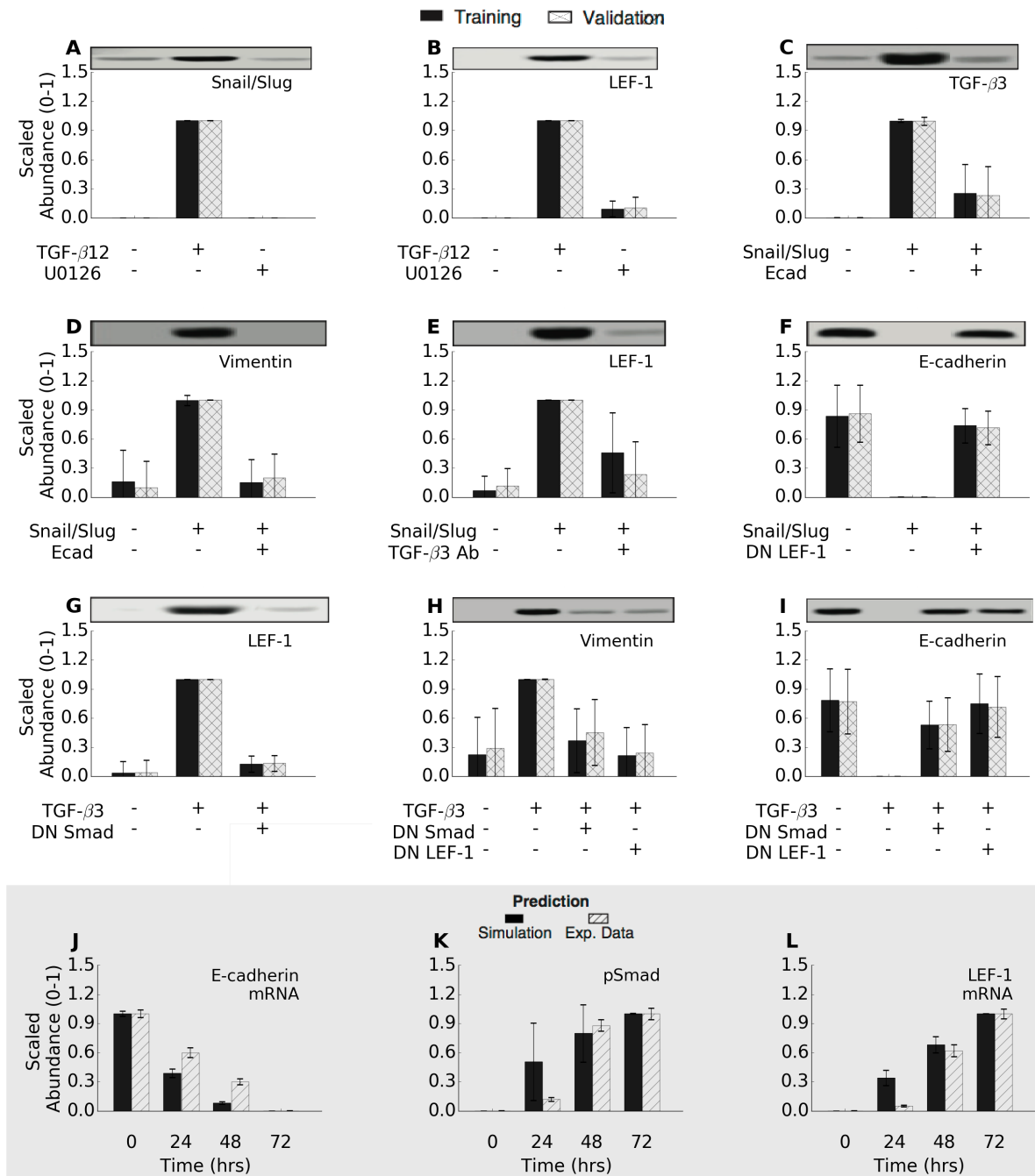


Fig. 2: Training and validation simulations. The population of EMT models qualitatively captured TGF- β -induced EMT signaling. (A-I) The population was generated using JuPOETs and trained using 11 different objective functions (41 data sets) taken from Medici *et al.* (Medici *et al.*, 2008). The model captured the simulated experiments for all cases when compared to randomized controls. (J-L) The model populations were also compared against untrained temporal data to measure the effectiveness as a pure prediction.

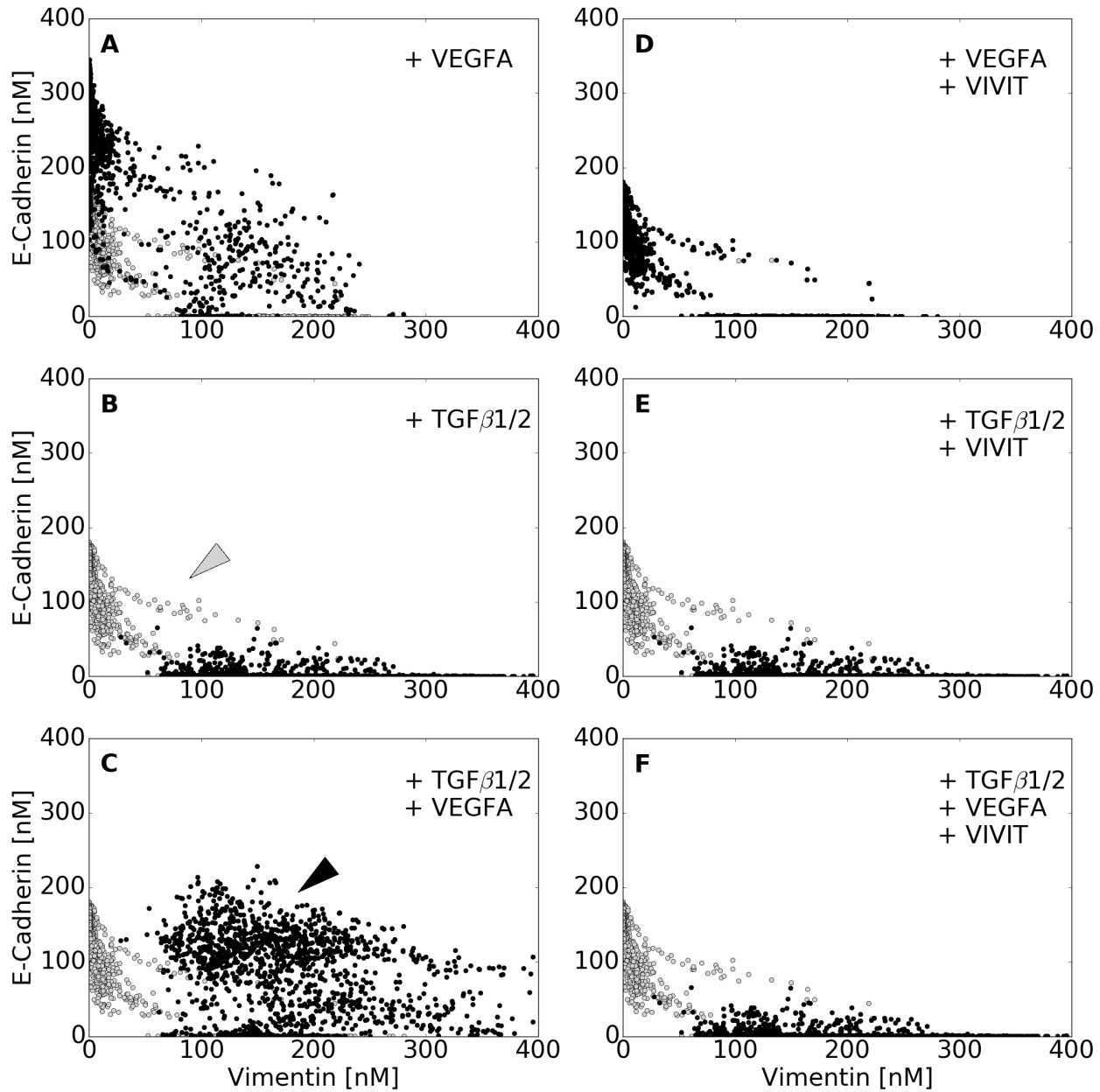


Fig. 3: Simulated VEGF-A and TGF- β 1/2 exposure promoted phenotype heterogeneity. Simulated response to TGF- β 1/2 and VEGF-A exposure with and without axis specific inhibitors. Vimentin and E-cadherin abundances (in nM) were used to quantify the shift in population at 48 hrs. (A-C) VEGF-A (50 a.u.) treatment resulted in a population with enhanced epithelial properties. This was contrary to the addition of TGF- β 2 (10 a.u.), which shifted the population towards a mesenchymal phenotype. Interestingly, the combined effects of TGF- β 2 and VEGFA was found to increase both ecadherin and vimentin levels, creating a heterogeneous population (black arrow), which can also be seen in a minority of untreated cells (gray arrow). (D-F) To isolate the effect of NFAT, we inhibited NFAT de-phosphorylation in combination with VEGFA. This negated the increase in ecadherin expression and shifted the population towards a mesenchymal phenotype. Likewise, combining NFAT inhibition with TGF- β mitigated all VEGF enhanced ecadherin expression. Lastly, combination of TGF- β 2, VEGFA, and NFAT inhibition nearly mitigated all effects of VEGFA, shifting the heterogeneous population towards a mesenchymal phenotype. In whole, high levels of phosphorylated-Sp1 correlated with vimentin expression, while NFAT was responsible for maintaining E-cadherin expression in the presence of other factors, although neither were mutually exclusive.

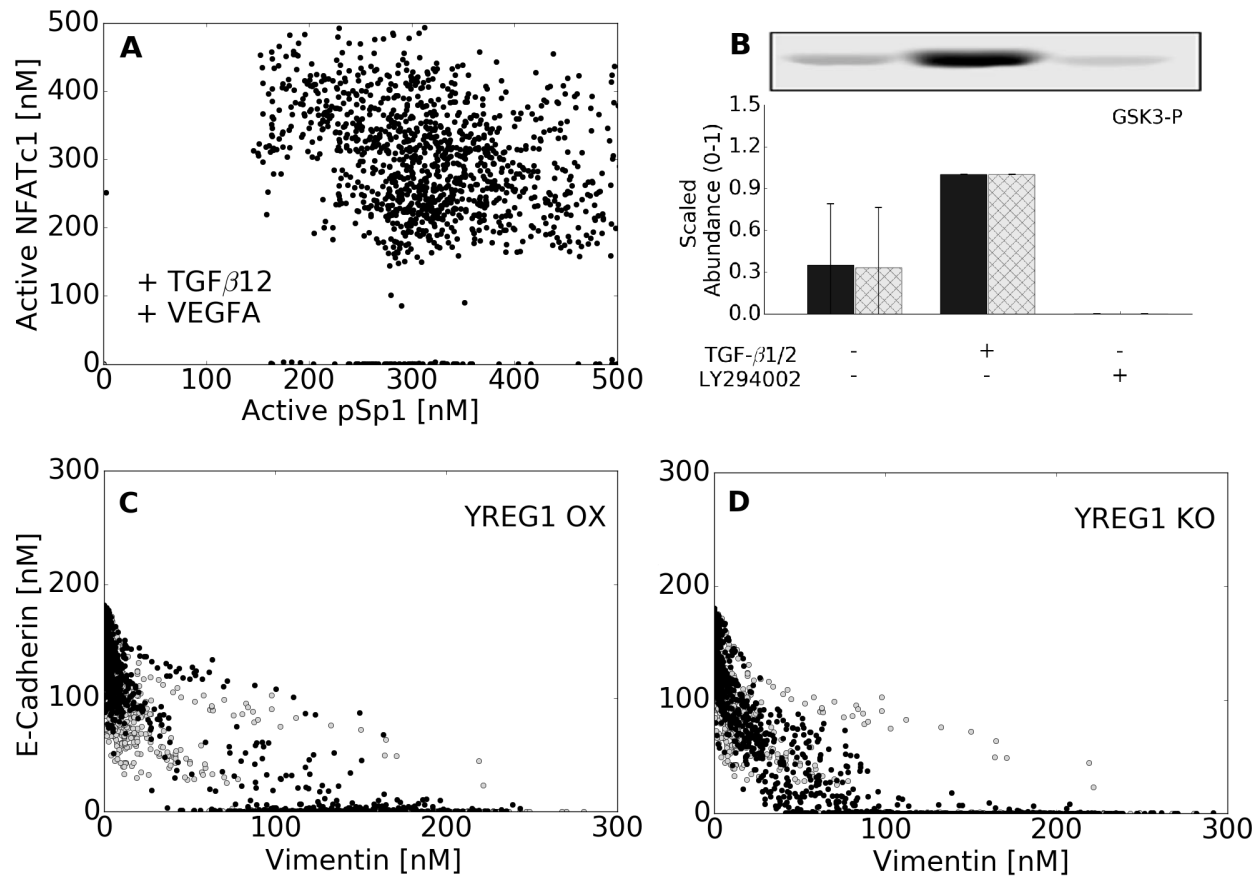


Fig. 4: Analysis of underlying signaling responses. (A) We examined the distribution of NFATc1 and AP1/SP1 in cells containing the hybrid phenotype (VEGF-A + TGF- β 2 case), showing the potential for cells to express both SP1 and NFATc1 in a non exclusive manner. (B) We were able to show a fit to an additional objective demonstrating the activation of GSK3 through PI3K. Our model captures this activation through TGF- β 3 signaling. LY294002 is a PI3K inhibitor. (C) We identified a novel regulator of LEF1 called YREG1 that allows Snail/Slug to emulate an inducer by repressing YREG1, which was required to stabilize the untreated population. YREG1 overexpression revealed an enhanced epithelial phenotype, while some inherently transformed cells moved towards a hybrid phenotype. (D) In the absence of YREG1, most of the population failed to consistently retain a stable epithelial state.

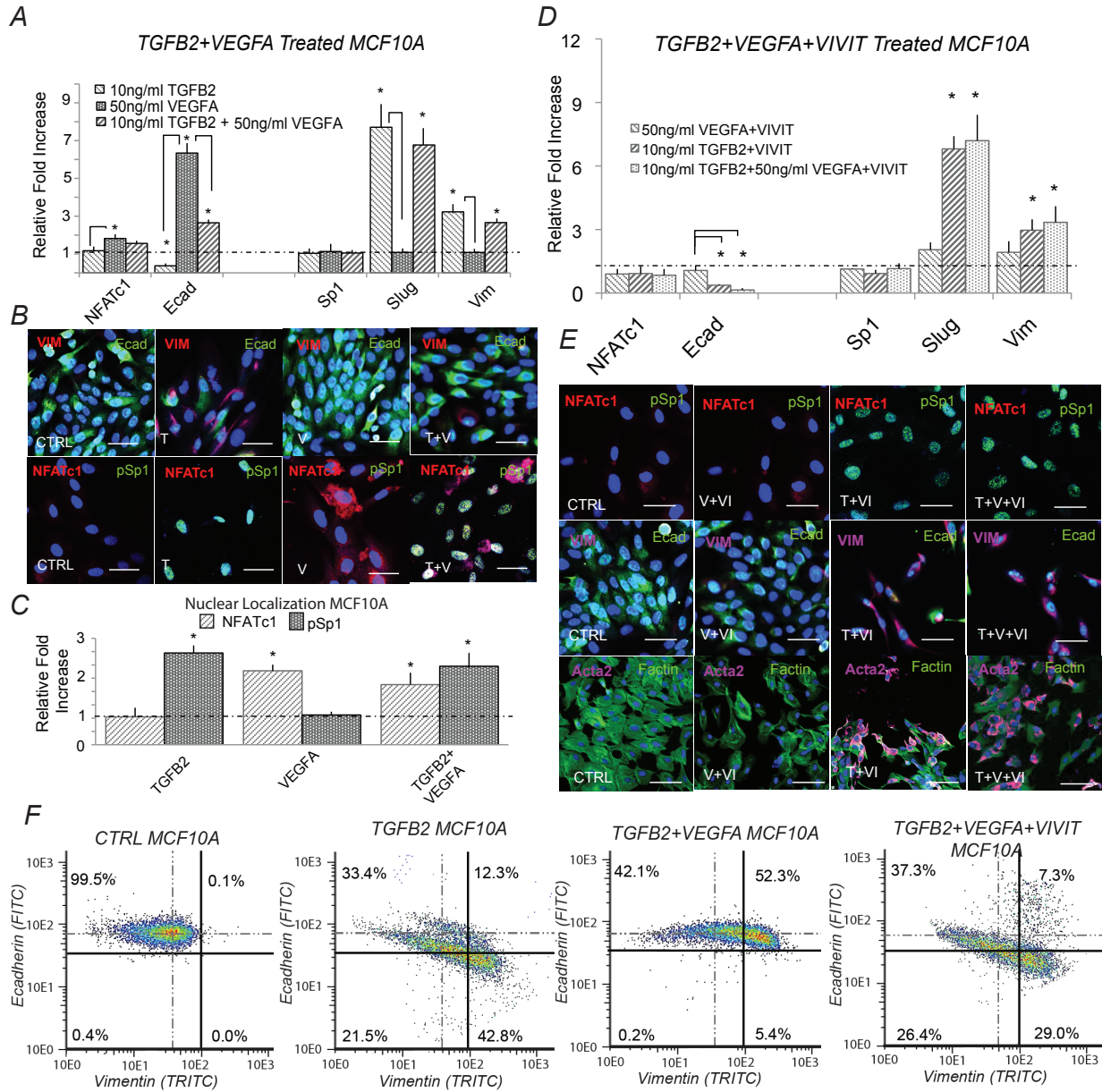


Fig. 5: Simultaneous TGF- β 1/2 and VEGF-A treatment induced phenotype heterogeneity and is dependent upon NFAT activity *in-vitro*. (A) In MCF10A, treatment with (10ng/ml) TGF- β 2 increased Slug and vimentin, while ecadherin expression was inhibited at both the gene and protein level at 48 hrs. Conversely, VEGFA alone increased both NFATc1 and ecadherin gene expression. Simultaneous TGF- β 2 (10ng/ml) and VEGFA (50ng/ml) treatment increased Slug, NFATc1, and vimentin expression, while also increasing ecadherin levels via qPCR. (B-C) Immunofluorescence confirmed these results and nuclear co-localization of both phospho-Sp1 and NFAT were found dependent upon TGF- β 2 and VEGFA, respectively. (D) To isolate the effect of NFAT, treatment of VEGFA (50ng/ml) and VIVIT (10 μ M) reduced ecadherin expression at 48hrs (control-dashed line). Similarly, combined TGF- β 2, VEGFA and VIVIT treatment increased Slug and vimentin expression, while inhibiting ecadherin levels via qPCR. (E) These findings were confirmed via immunofluorescence as the VIVIT peptide inhibited ecadherin and nuclear localization of NFATc1 in all three cases. (F) Quantitative flow cytometry also confirmed this trend. Similar experiments in DLD1 followed a similar trend (supplement). Magnification, 40x. Scale bars: 50 μ m. C=Control, T=TGF- β 2 , V=VEGFA, VI= NFAT inhibitor (VIVIT). Asterisks signify statistical differences from each other according to a one-way ANOVA with Tukey's post hoc ($p < 0.05$).

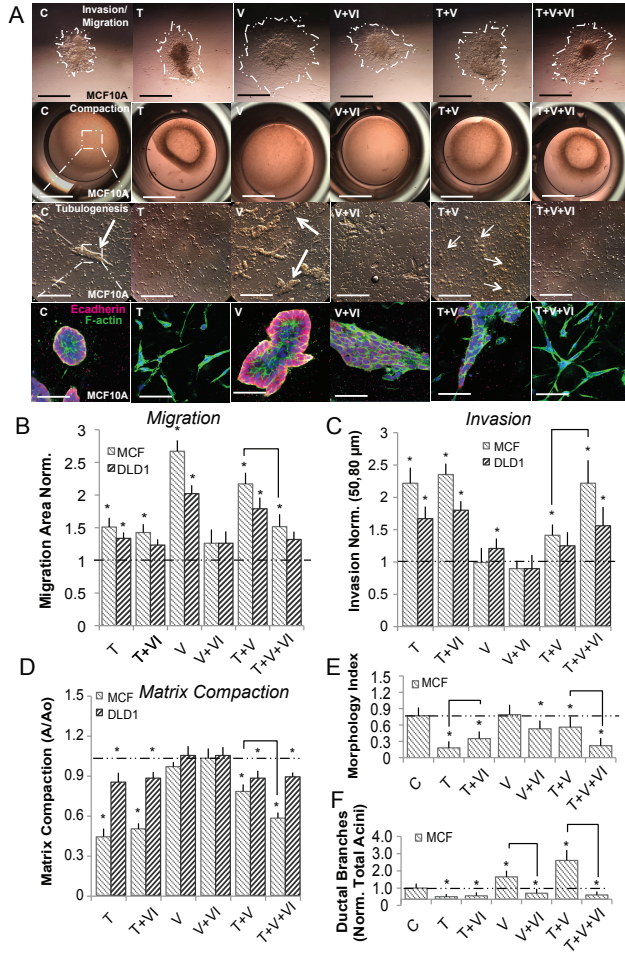


Fig. 6: Ductal branching is dependent upon phenotype heterogeneity within MCF10A in 3-D culture. MCF10A and DLD1 were formed into spheroids overnight and explanted to a collagen gel for 72 hrs. For compaction and tubular assays, cells were embedded into collagen gels for 72 hrs, and the extent of tubulogenesis was measured at 7 days. (A-D) Within MCF10A, TGF- β 2 (10ng/ml) enhanced invasion and contractile properties while, VEGFA (50ng/ml) promoted increased migration. TGF- β 2 with VEGFA significantly increased migration, while limiting with compaction. VIVIT (10 μ M) in combination with VEGFA and TGF- β 2 decreased migration and compaction, while increasing invasion. (D) Likewise, cell morphology (circularity index) correlated with both invasion and compaction in MCF10A. (E-F) The size of tubular structures (acini) also increased significantly upon addition of VEGFA, while the number of ductal branches was most significant upon simultaneous TGF- β 2 and VEGFA treatment (Red-Ecadherin, Green-Factin, Blue-Nuclear). DLD1 cells followed a similar trend, although the degree of migration, invasion, and compaction was less significant. In addition, no tubular structures were identified during the 7 day tubulogenesis endpoints. Scale bars: 500 μ m, 1000 μ m, 250 μ m, and 80 μ m, respectively. C=Control, T=TGF- β 2 , V=VEGFA, VI= NFAT inhibitor (VIVIT). Asterisks signify statistical differences from each other according to a one-way ANOVA with Tukey's post hoc ($p < 0.05$). Boxes in the left-most panel identify regions identified by arrows that were then imaged in greater zoom in the panel immediately below. The box diagram was not repeated for arrows in the other panels for clarity, but the same method was applied.

Supplemental Materials and Methods

Characteristic transcription and translation parameters. We used literature based transcription and translation parameters to establish the characteristic synthesis and degradation rates for both mRNA and protein. We estimated values for the rate parameters from the Bionumbers database (Milo *et al.*, 2010). These parameters were then used for all gene expression calculations:

```
-----  
# Description  
-----  
  
cell_diameter = 12 # \mu m  
number_of_rnapII = 75000 # copies/cells  
number_of_ribosome = 1e6 # copies/cells  
mRNA_half_life_TF = 2 # hrs  
protein_half_life = 10 # hrs  
doubling_time = 19.5 # hrs  
max_translation_rate = 5 # aa/sec  
max_transcription_rate = 6.0 # nt/sec  
average_transcript_length = 15000 # nt  
average_protein_length = 5000 # aa  
fraction_nucleus = 0.49 # dimensionless  
av_number = 6.02e23 # number/mol  
avg_gene_number = 2 # number of copies of a gene  
-----  
  
-----  
# Description  
-----  
  
# Calculate the volume (units: L)  
V = ((1-fraction_nucleus)*(1/6)*(3.14159)*(hl60_diameter)^3)*(1e-15)  
  
# Calculate the rnapII_concentration and ribosome_concentration (units: nM)  
rnapII_concentration = number_of_rnapII*(1/av_number)*(1/V)*1e9  
ribosome_concentration = number_of_ribosome*(1/av_number)*(1/V)*1e9  
  
# degradation rate constants (units: hr^-1)  
degradation_constant_mRNA = -(1/mRNA_half_life_TF)*log(0.5)  
degradation_constant_protein = -(1/protein_half_life)*log(0.5)  
  
# kcats for transcription and translation (units: hr^-1)  
kcat_transcription = max_transcription_rate*(3600/average_transcript_length)  
kcat_translation = max_translation_rate*(3600/average_protein_length)  
  
# Maximum specific growth rate (units: hr^-1)  
maximum_specific_growth_rate = (1/doubling_time)*log(2)  
  
# What is the average gene concentration (units: nM)  
avg_gene_concentration = avg_gene_number*(1/av_number)*(1/V)*1e9  
  
# Cell death constant (units: hr^-1)  
death_rate_constant = 0.2*maximum_specific_growth_rate
```

```

# Saturation constants for translation and transcription (units: nM)
saturation_transcription = 4600*(1/av_number)*(1/V)*1e9
saturation_translation = 100000*(1/av_number)*(1/V)*1e9
-----
```

Estimation and cross-validation of EMT model parameters. We used the Pareto Optimal Ensemble Technique (POETs) multiobjective optimization framework in combination with leave-one-out cross-validation to estimate an ensemble of TGF- β /EMT models. Cross-validation was used to calculate both training and prediction error during the parameter estimation procedure (Kohavi, 1995). The 41 intracellular protein and mRNA data-sets used for identification were organized into 11 objective functions. These 11 objective functions were then partitioned, where each partition contained ten training objectives and one validation objective. POETs integrates standard search strategies e.g., Simulated Annealing (SA) or Pattern Search (PS) with a Pareto-rank fitness assignment (Bassen *et al.*, 2016, Song *et al.*, 2010). Denote a candidate parameter set at iteration $i + 1$ as \mathbf{k}_{i+1} . The squared error for \mathbf{k}_{i+1} for training set j was defined as:

$$E_j(\mathbf{k}) = \sum_{i=1}^{\mathcal{T}_j} \left(\hat{\mathcal{M}}_{ij} - \hat{y}_{ij}(\mathbf{k}) \right)^2 \quad (\text{S1})$$

The symbol $\hat{\mathcal{M}}_{ij}$ denotes scaled experimental observations (from training set j) while \hat{y}_{ij} denotes the scaled simulation output (from training set j). The quantity i denotes the sampled time-index and \mathcal{T}_j denotes the number of time points for experiment j . In this study, the experimental data used for model training was typically the band intensity from Western or Northern blots. Band intensity was estimated using the ImageJ software package (Abramoff *et al.*, 2004). The scaled measurement for species x at time $i = \{t_1, t_2, \dots, t_n\}$ in condition j is given by:

$$\hat{\mathcal{M}}_{ij} = \frac{\mathcal{M}_{ij} - \min_i \mathcal{M}_{ij}}{\max_i \mathcal{M}_{ij} - \min_i \mathcal{M}_{ij}} \quad (\text{S2})$$

O#	Species (protein)	Cell Type	Training	Prediction	Random
O1	LEF1	DLD1 CC,MDCKII,A375 MC	0.54 ± 0.167	0.505 ± 0.175	1.765 ± 0.223
O2	Vimentin	DLD1 CC,MDCKII,A375 MC	1.044 ± 0.668	0.783 ± 0.666	2.098 ± 0.784
O3	TGF β 3	DLD1 CC,MDCKII,A375 MC	0.119 ± 0.262	0.225 ± 0.418	1.408 ± 0.732
O4	E-cadherin	DLD1 CC,MDCKII,A375 MC	2.299 ± 0.449	2.154 ± 0.625	3.459 ± 0.643
O5	β -catenin	DLD1 CC,MDCKII,A375 MC	0.752 ± 0.38	0.514 ± 0.351	1.025 ± 0.0
O6	TGF β 3	DLD1 CC,MDCKII,A375 MC	1.662 ± 0.55	1.54 ± 0.677	3.328 ± 0.981
O7	GSK3-P	DLD1 CC,MDCKII,A375 MC	0.19 ± 0.291	0.203 ± 0.292	0.756 ± 0.309
O8	LEF1	DLD1 CC,MDCKII,A375 MC	0.023 ± 0.078	0.03 ± 0.11	0.937 ± 0.298
O9	E-Cadherin	DLD1 CC,MDCKII,A375 MC	1.092 ± 1.228	1.412 ± 1.348	2.652 ± 1.435
O10	Snail/Slug	DLD1 CC,MDCKII,A375 MC	0.019 ± 0.0	0.019 ± 0.0	1.111 ± 0.744
O11	LEF1	DLD1 CC,MDCKII,A375 MC	0.005 ± 0.015	0.013 ± 0.06	0.797 ± 0.431

Fig. S1: Training and prediction values as a function of condition for the 11 TGF- β objective functions versus a random parameter control.

Under this scaling, the lowest intensity band equaled zero while the highest intensity band equaled one. A similar scaling was defined for the simulation output. By doing this scaling, we trained the model on the relative change in blot intensity, over conditions or time (depending upon the experiment). Thus, when using multiple data sets (possibly from different sources) that were qualitatively similar but quantitatively different e.g., slightly different blot intensities over time or condition, we captured the underlying trends in the scaled data. JuPOETs is free or charge, open source and available for download under an MIT software license from <http://www.varnerlab.org>. Details of the JuPOETs implementation, including example codes are presented in Bassen *et al.*, (Bassen *et al.*, 2016).

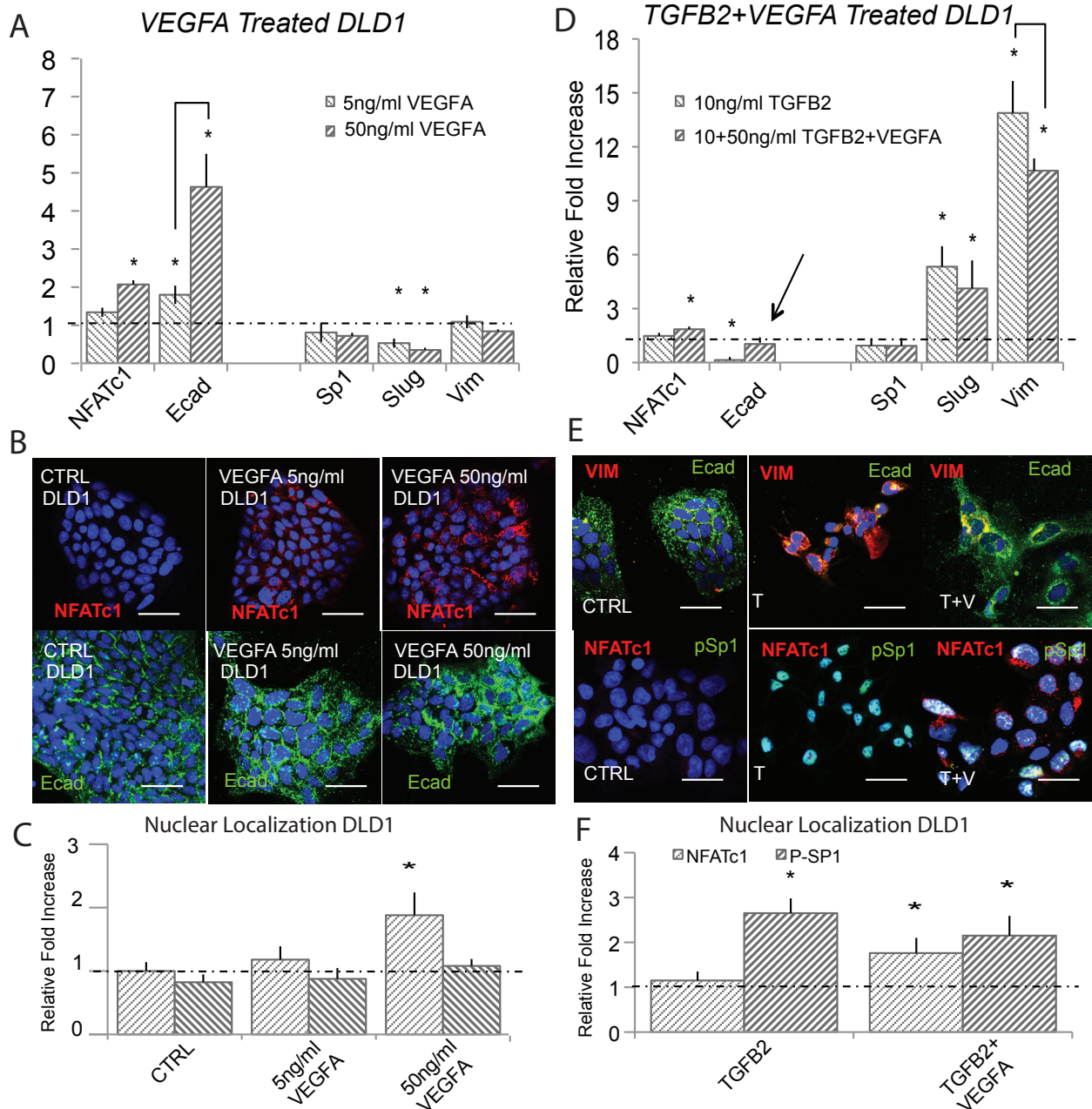


Fig. S2: VEGF-A attenuates TGF- β 1/2 to induce phenotype heterogeneity in DLD1. (A) In DLD1, we found that 5ng/ml of VEGFA increased NFATc1 and E-cadherin gene expression via qPCR and 50ng/ml potentiated this effect at 48 hrs. (B - C) These findings were confirmed at the protein level via immunofluorescence, as ecadherin levels and nuclear localization of NFATc1 increased. (D) Treatment with (10ng/ml) TGF β 2 resulted in mesenchymal transformation as measured via qPCR against target genes Slug, ecadherin, vimentin, Sp1, and NFATc1. (E - F) Immunofluorescence and nuclear localization revealed a strong presence of phospho-Sp1. (G) Combination of VEGFA (50ng/ml) and TGF β 2 (10ng/ml) treatment resulted in increased Slug, NFATc1, and vimentin expression, while also increasing ecadherin levels compared to control. (H) Immunofluorescence confirmed these results, as both ecadherin and vimentin levels were elevated. (I) A significant increase in nuclear localization of both NFATc1 and phospho-Sp1 were also found. Magnification, 40x. Scale bars: 50 μ m. C=Control, T=TGF β 2 , V=VEGFA, VI=NFAT inhibitor (VIVIT). Asterisks signify statistical differences from each other according to a one-way ANOVA with Tukey's post hoc ($p < 0.05$).

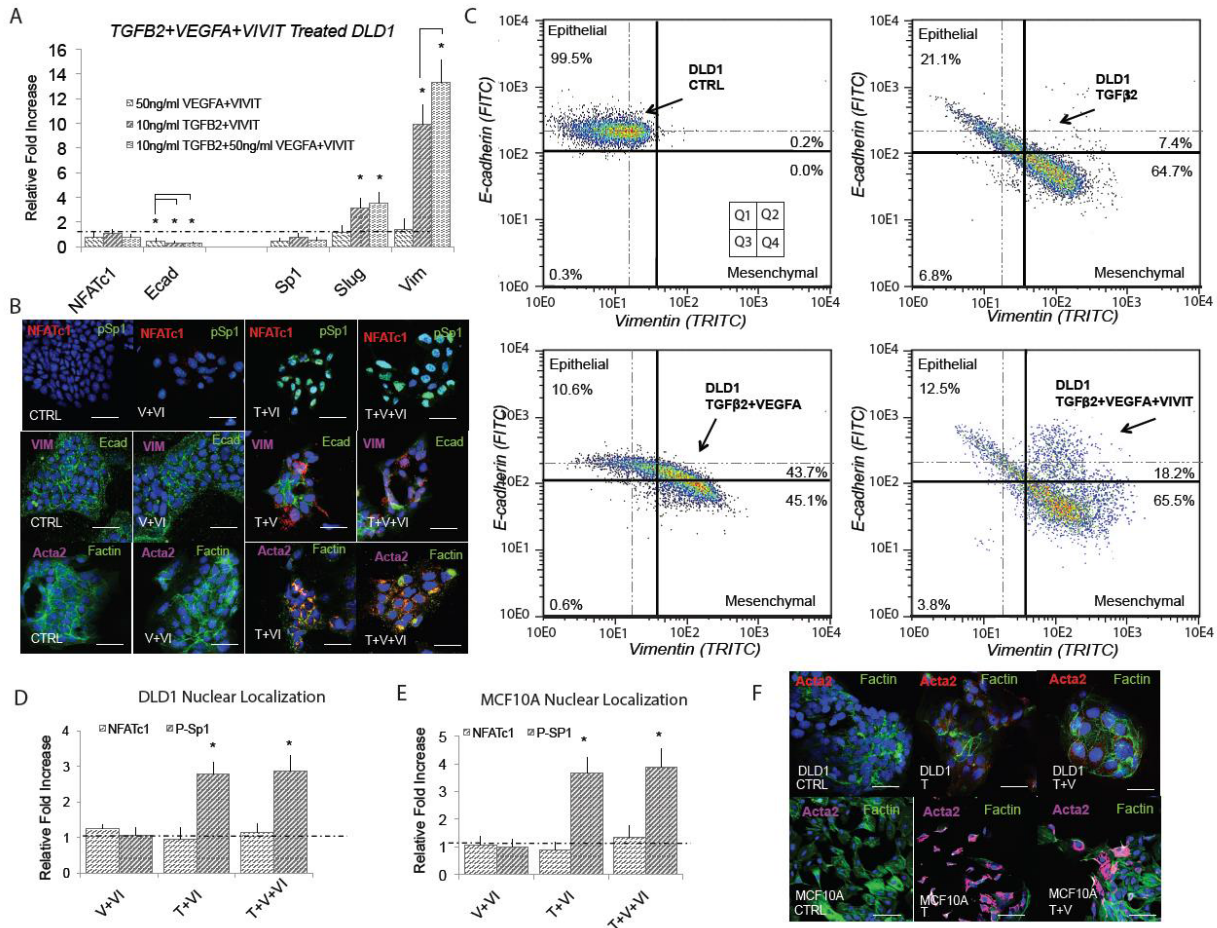


Fig. S3: E-cadherin expression is dependent upon NFAT activity in DLD1. (A) Treatment with VEGFA (50ng/ml) and NFAT inhibitory peptide VIVIT (10μM) resulted in significantly reduced ecadherin expression (qRT-PCR at 48hrs). Addition of TGF β 2 (10ng/ml) and VIVIT resulted in increased Slug and vimentin expression, while inhibiting ecadherin levels. Combined TGF β 2, VEGFA, and VIVIT treatment resulted in target genes Slug and vimentin expression increased, while inhibiting ecadherin levels. No change in Sp1 or NFATc1 expression was found. (B) These findings were confirmed via immunofluorescence as the VIVIT inhibitors was shown to inhibit ecadherin levels in all three cases. We also found no change in gene or nuclear localization of NFATc1 in all three cases, while phospho-Sp1 was found to increase in both TGF β conditions. (C) Quantitative flow cytometry also confirmed this trend. (D,E) TGF β 2, VEGFA and VIVIT treatment in DLD1 and MCF10A resulted in no change of Sp1 expression or NFATc1 expression. (F) Likewise, no change in nuclear localization of NFAT in all three cases, however phospho-Sp1 was found to increase in both TGF β conditions. Magnification, 40x. Scale bars: 50μm. C=Control, T=TGF β 2 , V=VEGFA, VI= NFAT inhibitor (VIVIT). Asterisks signify statistical differences from each other according to a one-way ANOVA with Tukey's post hoc ($p < 0.05$).

PRELIMINARY DATA USED TO HANDFIT RESPONSE OF VEGFA WITHIN SYSTEM

		MCF10A						
VEGFA		Relative mRNA			Normalized			
		Ecad	Slug	Vim	Ecad	Slug	Vim	
	5ng/ml	3HR	1.31	1.04	0.93	0.00	1.00	1.00
		48 HR	3.60	1.03	0.91	0.45	0.94	0.88
50ng/ml		3HR	1.37	0.92	0.88	0.01	0.25	0.71
		48 HR	6.34	0.88	0.76	1.00	0.00	0.00
Standard Deviation								
VEGFA		Relative mRNA			Normalized			
		Ecad	Slug	Vim	Ecad	Slug	Vim	
		5ng/ml	0.89	0.03	0.02	0.00	0.03	0.02
50ng/ml		3HR	0.78	0.03	0.27	0.10	0.03	0.26
		48 HR	0.11	0.10	0.53	0.00	0.03	0.43
VEGFA		Relative mRNA			Normalized			
		Ecad	Slug	Vim	Ecad	Slug	Vim	
5ng/ml		3HR	1.21	0.76	1.03	0.00	1.00	0.76
		48 HR	1.80	0.53	1.09	0.17	0.44	1.00
50ng/ml		3HR	1.54	0.46	1.03	0.10	0.27	0.76
		48 HR	4.63	0.35	0.84	1.00	0.00	0.00
Standard Deviation								
VEGFA		Relative mRNA			Normalized			
		Ecad	Slug	Vim	Ecad	Slug	Vim	
		5ng/ml	0.80	0.10	0.18	0.00	0.13	0.13
50ng/ml		3HR	0.24	0.12	0.17	0.02	0.10	0.16
		48 HR	0.89	0.19	0.45	0.06	0.11	0.33
VEGFA		Absolute mRNA			Normalized			
		Ecad	Slug	Vim	Ecad	Slug	Vim	
5ng/ml		3HR	0.94	88.12	10.23	0.00	1.00	1.00
		48 HR	2.10	55.64	5.45	0.40	0.41	0.40
50ng/ml		3HR	1.44	64.10	8.43	0.17	0.56	0.77
		48 HR	3.85	33.40	2.32	1.00	0.00	0.00
Standard Deviation								
VEGFA		Absolute mRNA			Normalized			
		Ecad	Slug	Vim	Ecad	Slug	Vim	
		5ng/ml	0.21	22.34	2.45	0.00	0.25	0.24
50ng/ml		3HR	0.45	15.55	1.12	0.09	0.11	0.08
		48 HR	0.38	17.87	2.23	0.05	0.16	0.20
VEGFA		3HR	1.30	9.46	0.45	0.34	0.00	0.00

Fig. S4: VEGF-A qPCR data used to hand fit VEGF enhancement of E-cadherin expression. mRNA was harvested after 3hr and 24hr timepoint.